

# Review Article

## Application of MRS to mouse models of neurodegenerative illness

Ji-Kyung Choi,<sup>1</sup> Alpaslan Dedeoglu<sup>2</sup> and Bruce G. Jenkins<sup>1\*</sup>

<sup>1</sup>Department of Radiology, Athinoula A. Martinos Center for Biomedical Imaging, Massachusetts General Hospital and Harvard Medical School, Charlestown, MA, USA

<sup>2</sup>Department of Neurology, Boston University School of Medicine, Bedford VA Medical Center, Bedford, MA, USA

Received 15 September 2006; Revised 5 December 2006; Accepted 9 December 2006

**ABSTRACT:** The rapid development of transgenic mouse models of neurodegenerative diseases, in parallel with the rapidly expanding growth of MR techniques for assessing *in vivo*, non-invasive, neurochemistry, offers the potential to develop novel markers of disease progression and therapy. In this review we discuss the interpretation and utility of MRS for the study of these transgenic mouse and rodent models of neurodegenerative diseases such as Alzheimer's (AD), Huntington's (HD) and Parkinson's disease (PD). MRS studies can provide a wealth of information on various facets of *in vivo* neurochemistry, including neuronal health, gliosis, osmoregulation, energy metabolism, neuronal–glial cycling, and molecular synthesis rates. These data provide information on the etiology, natural history and therapy of these diseases. Mouse models enable longitudinal studies with useful time frames for evaluation of neuroprotection and therapeutic interventions using many of the potential MRS markers. In addition, the ability to manipulate the genome in these models allows better mechanistic understanding of the roles of the observable neurochemicals, such as *N*-acetylaspartate, in the brain. The argument is made that use of MRS, combined with correlative histology and other MRI techniques, will enable objective markers with which potential therapies can be followed in a quantitative fashion. Copyright © 2007 John Wiley & Sons, Ltd.

**KEYWORDS:** MRS; *N*-acetylaspartate; neurodegenerative disease; Alzheimer's disease; Huntington's disease; Parkinson's disease; transgenic mice

### INTRODUCTION

Since its introduction for human study in the early 1980s, MR has proved to be an extremely versatile technique for evaluating many different parameters of anatomical, physiological, and metabolic interest. The number of phenomena amenable to analysis with MR techniques is increasing every year. This versatility arises from the many different sources of magnetic contrast that can be generated using either endogenous or exogenous contrast, from the versatility of the techniques for manipulation of the nuclear spins that generate the observed signals, and from the extremely safe nature of MR which lends itself to longitudinal studies and large patient populations.

\*Correspondence to: B. G. Jenkins, Building 149, 13th Street, Charlestown, MA 02129, USA.  
E-mail: bgj@nmr.mgh.harvard.edu

**Abbreviations used:** AD, Alzheimer's disease; ALS, amyotrophic lateral sclerosis; APP, amyloid precursor protein; Cho, choline; Cr, creatine; CSF, cerebrospinal fluid; GABA,  $\gamma$ -aminobutyric acid; HD, Huntington's disease; HPRT, hypoxanthine phosphoribosyltransferase; HRMAS, high-resolution magic angle spinning; htt, huntingtin; MPP<sup>+</sup>, *N*-methyl-4-phenylpyridinium; MPTP, 1-methyl-4-phenyl-1,2,3,6-tetrahydropyridine; NAA, *N*-acetylaspartate; PCr, phosphocreatine; PD, Parkinson's disease; PET, positron emission tomography; PS, presenilin; SNR, signal-to-noise ratio; TCA, tricarboxylic acid.

MR techniques can now evaluate tissue parameters relevant to tricarboxylic acid (TCA) cycle metabolism, anaerobic glycolysis, adenosine ATP concentrations, blood–brain barrier permeability, macrophage infiltration, cytotoxic edema, spreading depression, cerebral blood flow and volume, and neurotransmitter function. The paramagnetic nature of certain oxidation states of iron allows brain function to be mapped out using deoxyhemoglobin as an endogenous contrast agent; local tissue iron concentrations can also be assessed. In addition to these metabolic parameters, the number of ways to generate anatomical contrast using MR is also expanding, and, in addition to conventional anatomical scans, mapping of axonal fiber tracts can be performed using anisotropy of water diffusion. A selective, non-exhaustive, summary of the various parameters of relevance to neurodegeneration that can be measured using MR techniques is presented in Table 1. A schematic representing the 'phylogenetic tree' of MR techniques for chemical, physiological and structural purposes is shown in Fig. 1.

Current trends suggest that multimodal imaging approaches to a given neurobiological problem are likely to be more fruitful than a single tool such as MRS; however, space precludes a competent review of all these various techniques. Therefore, we will describe the use of

**Table 1. Parameters of relevance to neurodegeneration amenable to MR analysis**

Parameter and/or chemical	Relevance to neurodegeneration	MR techniques and/or parameters used	MR references
ATP	ATP defects noted in mitochondrial disorders	$^{31}\text{P}$ MRS	(143–145)
Lactate	Marker for impaired energy metabolism and/or reduced blood flow	$^1\text{H}$ MRS	(41,61,146)
Glucose	Can be used in labeled form ( $^{13}\text{C}$ ) to examine TCA cycle flux	$^{13}\text{C}$ MRS; $^1\text{H}$ MRS	(100,147,148)
Glutamate	Marker for potential excitotoxicity; in labeled form ( $^{13}\text{C}$ ) marker for TCA cycle metabolism	$^{13}\text{C}$ MRS; $^1\text{H}$ MRS	(70,100,149)
Glutamine	Marker for determination of neuronal/glial Glu/Gln cycling or ammonia toxicity	$^{13}\text{C}$ MRS; $^1\text{H}$ MRS	(101,150,151)
<i>N</i> -Acetylaspartate	Marker for neuronal number, integrity and health	$^1\text{H}$ MRS	(39,56,152)
<i>myo</i> -Inositol	Marker for glial cells and cerebral osmolarity	$^1\text{H}$ MRS	(35,77,78)
Phosphoesters	May be markers for neuronal membrane integrity	$^{31}\text{P}$ MRS	(81)
Macromolecular/lipid resonances	Potential markers for macrophage/microglial activity	$^1\text{H}$ MRS	(60,85)
Apparent diffusion coefficient	Markers for cytotoxic edema, vasogenic edema, cell swelling, and fiber tract mapping	Pulsed field gradient spin echoes	(153–156)
Blood–brain barrier permeability	Impairment during ischemia, tumors and possibly AD	Decreased $T_1$ after injection of contrast agents	(157,158)
Iron content	Can be used to look for evidence of increased iron in PD or fractional anisotropy (FA)	Mapping of $T_2^*$ and $T_2'$ relaxivity changes	(159–161)
Blood oxygenation level-dependent contrast	Marker for neuronal activity; can derive relative oxygen consumption.	Fast gradient echo, or asymmetric spin echo imaging	(162,163)
Cerebral blood flow and volume	Markers for tissue perfusion, neuronal and neurotransmitter activity	FAIR or arterial spin labeling ( $T_1$ -based), contrast injections ( $T_2^*$ -based)	(164–167)

References are non-exhaustive and weighted towards those of direct relevance to *in vivo* study of neurodegenerative disorders.

### Phylogenetic Tree of MR Techniques

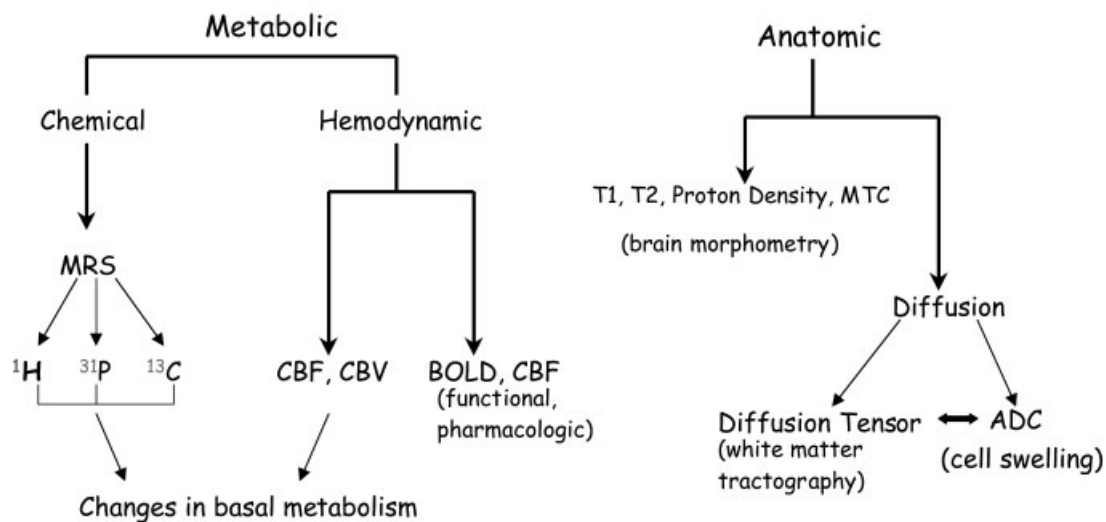


**Figure 1.** Schematic for the “phylogenetic tree” of various MR techniques. We have divided MR techniques into metabolic (including MRS and functional MRI) and anatomic techniques. The metabolic are further subdivided into those that measure hemodynamic or chemical parameters. The anatomic have been subdivided into those used for brain morphometry and those used for brain tractography. Obviously the cladistics are somewhat arbitrary.

MRS for examination of neurodegeneration and potential therapeutic strategies in transgenic mouse models of neurodegenerative illness. MRS techniques have much to offer for the evaluation of brain physiology, chemistry and function of neurodegenerative disorders. These types of study can generally be divided into three main areas: etiology, natural history and progression of the disease, and therapy. The development of transgenic mice has led to large increases in the efficiency of testing potential therapeutics and pathology in mouse models of neurodegeneration. A number of the models that have been developed closely replicate many of the symptoms and pathological features of the corresponding human disease, in spite of the large differences in lifespan between mice and humans. The great flexibility with which the mouse genome can be manipulated allows a number of fascinating questions about which aspects of a gene mutation is most lethal or deleterious to be answered. For instance, knockout of the native gene responsible for Huntington's disease (HD) is embryonic lethal (1), whereas expression of the HD mutation (an expanded CAG repeat) on another gene can lead to a completely different phenotype (2). The progress in generating and understanding these mouse models has been as rapid as the proliferation of MR techniques for understanding the brain, but the number of MRS studies of mouse models of neurodegeneration is still rather limited. We will summarize some of the data and concepts generated by studies of models of the most common neurodegenerative diseases.

Although a surprising convergence of evidence indicates that many neurodegenerative illnesses have a common mechanism of aberrant protein folding and aggregation (3–6), understanding disease progression and finding potential therapies are still quite difficult. This is not surprising, as many of the pathways leading to neuronal death are common and progressive. This results in what can be termed the 'neurodegenerative cascade'. We use the model of focal ischemia as an example because so much effort has gone into understanding this cascade. The initial insult in focal ischemia is clear, an interruption of blood flow, leading to cessation of ATP production. However, the cascade of events that results from this process is extremely complicated, and the ultimate neuronal destruction is a result of multiple interactive pathways. This is exemplified by the large number of different therapeutic approaches that prove efficacious in experimental ischemia. Aside from the obvious 'clot busting' therapies such as tissue plasminogen activator, effective reduction of final infarct size can be demonstrated using Glu antagonists (e.g. MK-801) to decrease excitotoxicity, inhibition of apoptosis using caspase inhibitors, trapping of free radicals using spin traps [e.g. *n*-*t*-butyl- $\alpha$ -(2-sulfophenyl) nitron] to block the negative consequences of excess free-radical production, energy repletion, calcium channel blockers to inhibit intracellular calcium influx, and the

list goes on [see reviews in (7–12)]. Each of these approaches targets one component of an interactive mesh. Similar observations have been made with a toxin model of neurodegeneration, acute *N*-methyl-4-phenylpyridinium (MPP<sup>+</sup>) toxicity, where the initial insult is impairment of ATP production via blockade of complex I in the electron transport chain, yet multiple therapeutic strategies are effective in ameliorating the lesions (13–15).

It is therefore easy to see why many deleterious factors observed in a neurodegenerative illness may be the result, rather than the cause, of a given disease. Once the neurodegenerative process has been initiated, other negative factors, associated with natural aging for instance, may accelerate it. Thus, questions need to be framed about the etiology in order to address both the primary insult itself and the secondary consequences of the primary insult that may lead to further progressive degeneration. The secondary consequences can be considered to be part of the 'natural history' of the disease. Such a parsing of primary, secondary and even tertiary effects with respect to energy metabolism has been proposed by Blass and colleagues (16). Irrespective of questions about etiology or natural history, the multiple factors involved in the 'neurodegenerative cascade' provide many potentially efficacious therapeutic entry points for either preventing or slowing down the neurodegenerative process. It is for this reason that the mouse models of neurodegeneration are so appealing, as they allow more efficient testing of potential therapies than could ever be attained in humans. Mice have much shorter lifespans allowing large numbers of animals to be tested in short time periods, and, further, environmental factors can be controlled with much more precision than with human studies. Indeed, many of therapeutic entry points have been tested in mouse models of neurodegeneration. Several mouse studies have used MRS to test either efficacy as a surrogate end point (17) or mechanistic aspects, such as increases in brain creatine (Cr) associated with Cr therapy (18,19).

One of the most powerful features of MRI/MRS studies is that they allow interrogation of a problem at both the molecular and systems level. The various features amenable to analysis using various MR techniques are outlined in Table 1. Elements of this story have also been reviewed in animal models (20). A brief summary of results from rodent models of neurodegeneration is presented in Table 2.

## EVALUATION OF NEUROCHEMISTRY

MRS is one of the few available techniques that can provide *in vivo* information on neurochemistry non-invasively. It is extremely versatile with respect to the many chemicals and brain processes that can be examined, as seen in Table 1. A number of different

**Table 2. Summary of MRS in animal models of neurodegenerative diseases**

Disease	Summary	References
HD	<i>In vivo</i> MRS in transgenic mice (R6/1 line): reduced NAA (26%) in the corpus striatum at 5 months of age; cholines and Cr/phosphocreatine not altered	(135)
HD	MAS <sup>1</sup> H MRS in R6/2 mice: lower levels of NAA, GABA, Asp, Ala, acetate, choline and phosphocholine in decreasing order of significance (from striatum). Raised levels of glycerophosphocholine, <i>scyllo</i> -inositol, Gln, taurine, <i>myo</i> -inositol, lactate and Cr in decreasing order of significance	(138)
HD	2% Cr administration (R6/2): attenuated reductions in striatal NAA assessed by MRS	(18)
HD	MRS in Cr-supplemented mice (R6/2): increased brain Cr concentration and delayed decreases in NAA concentration	(19)
HD	MRS in CGS21680-treated mice (R6/2): CGS reduced the increased choline concentrations in the striatum	(17)
HD	Chronic 3-nitropropionic acid (3NP) treatment: a region-selective increase in lactate was detected in the striatum and a progressive and region-specific decrease in striatal NAA, Cr, and choline occurring as early as 3 weeks before the first detection of lactate	(168)
HD	R6/2 mice (mutant htt with 141 CAG repeat): 53% fall in NAA, large increase in glucose (600%) ( <i>in vivo</i> ). <i>In vivo</i> and <i>in vitro</i> shows increases in Gln (100%), taurine (95%), cholines (200%), <i>scyllo</i> -inositol (333%) and decreases in Glu (24%), succinate (47%).	(39)
HD	3NP injection in rat: chemical shift imaging (CSI) measurement showed raised lactate in the striatum and decreased NAA	(15)
PD	MPP <sup>+</sup> injection in rat: CSI measurement showed raised lactate in the striatum and decreased NAA	(15)
PD	Long-term neurodegenerative and bioadaptive neurochemical changes in a primate model (14 ± 5 months): 23-fold increase in lactate and macromolecules in the striatum region of the brain for up to 10 months after the last administration of MPTP but returned to normal level by 2 years after MPTP	(140)
PD	MPTP-treated mice: NAA was significantly diminished in the substantia nigra pars compacta and striatum	(141)
PD	MPTP-treated C57BL/6 mice: marked increases in lactate/Cr ratio were observed at 2 h and then quickly returned to about basal level by 7 h after injection of MPTP	(169)
PD	MPP <sup>+</sup> injection in rat: CSI showed a marked increase in striatal lactate and a depletion of ATP up to 48 h after the injections	(115)
MND/ALS	Mutant wobbler mice: the ratio of NAA to total Cr was significantly lower in affected mice (0.79 ± 0.05) vs 0.98 ± 0.10	(170)
ALS	SOD1 (G93A) mice: <i>in vivo</i> MRS showed significantly increase cortical Glu at 115 days. Creatine attenuated the increase in Glu at 75 days of age but no effect at 115 days	(71)
AD	Mice (APPTg2576) <i>in vivo</i> and <i>in vitro</i> MRS: decreases in NAA (17%), Glu (22%), glutathione (36%) in the cerebral cortex at 19 months. Increase in taurine (21%), but not <i>myo</i> -inositol.	(122)
AD	APP × PS1 mice: a reduction in the concentrations of NAA and Glu compared with total Cr with advancing age. A dramatic increase in <i>myo</i> -inositol with age.	(86)
AD	APP × PS2 mice: <i>in vivo</i> MRS showed significantly reduced NAA and Glu in the older animals. NAA concentrations correlated with plaque area. No change in inositol	(123)

nuclei can be observed using MR, and those that are most commonly seen in brain disorders (in decreasing order of number of studies) are <sup>1</sup>H, <sup>31</sup>P, <sup>13</sup>C, <sup>19</sup>F, <sup>15</sup>N, <sup>23</sup>Na, and <sup>7</sup>Li, with the first three accounting for approximately 99% of all studies. Although only <sup>1</sup>H and <sup>31</sup>P have been applied extensively to neurodegenerative conditions, a number of potential studies of neurodegeneration could be performed using either <sup>13</sup>C and <sup>23</sup>Na. With <sup>13</sup>C, TCA cycle dynamics can be assayed, and the efficacy of a given neuroprotective compound in improving cellular energetics determined. On the other hand, <sup>23</sup>Na may be useful for examining changes in intracellular and extracellular sodium content during a stroke (21–24).

Because of its sensitivity, <sup>1</sup>H MRS is the most common application in brain. At lower field strengths such as 1.5 T and even 3 T, the number of chemicals that can be reliably quantified is relatively low, including lactate (if present), *N*-acetylaspartate (NAA), Glx (Glu plus Gln), Cr/

phosphocreatine (PCr), trimethylamine (choline)-containing compounds, *myo*-inositol, and, in the rodent brain, taurine (in primate brain, not much taurine is routinely observed, whereas in rodent brain taurine concentrations are quite high at about 5 mM). The current large impetus for higher field strengths doubly benefits MRS (as opposed to MRI) because of the increase in signal-to-noise ratio (SNR) coupled with the increase in spectral dispersion, leading to much easier identification of many overlapping resonances.

At much higher field strengths, such as 7 T in humans and 9.4 T in animals, it is possible to quantify even more chemicals (25,26). As an example, we show the ultimate in neurochemical detection: *in vitro* MRS spectra of brain extracts at high field. Figure 2 shows a spectrum from a mouse at 600 MHz (14 T). The assignments of the resonances can be found in numerous sources (27–29). It is clear that many chemicals can be detected. A brief

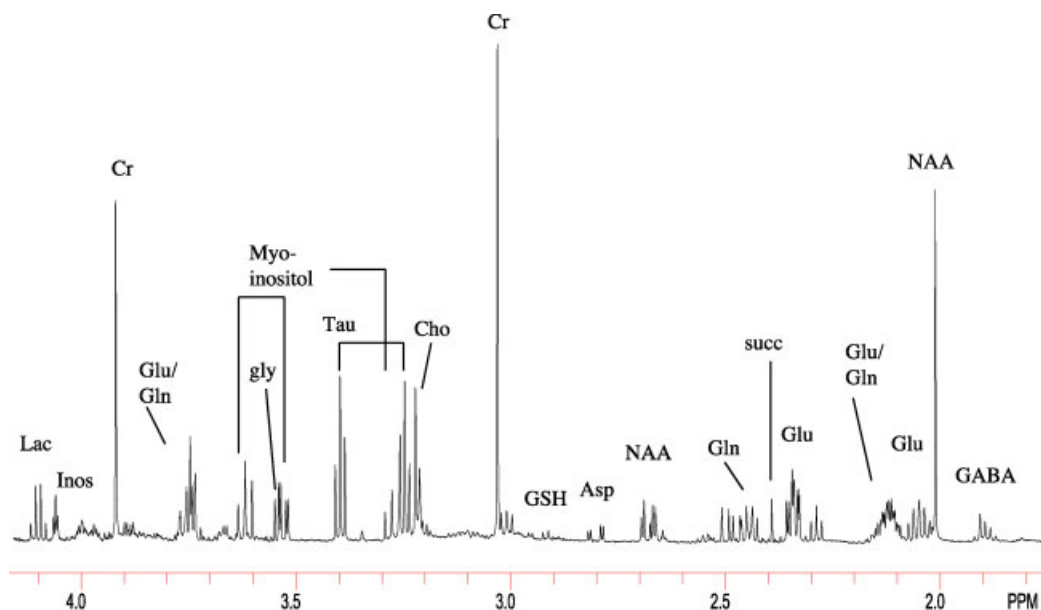


**Figure 2.** Spectra from a brain extract of a wild-type mouse taken at 600 MHz (14 T). The high field strength provides excellent spectral dispersion and discrimination of many different neurochemicals.  $TR$  in this spectrum is 10 s, so the peak areas are proportional to concentration directly after correction for the number of protons giving rise to a particular resonance.

synopsis of the relevance of the major neurochemicals, and their utility as markers for neurodegeneration and neuroprotection, is given below.

### N-Acetylaspartate

There seems to be little doubt that NAA is a marker for neurons because it is found almost exclusively in neurons but not in glial cells (30–33). The concentration of NAA is spatially fairly uniform within both gray and white matter, with the major distinction that neurons with extensive axonal projections, such as in the substantia nigra, have higher concentrations than those with shorter projections, such as in the striatum. NAA concentration seems to be similar in the major neurotransmitter neuronal subtypes, including cholinergic, noradrenergic, GABAergic ( $\gamma$ -aminobutyric acid) and Glutamatergic neurons (31). The biochemical literature indicates that NAA concentration is higher in gray matter than in white matter (by a factor of about 2) [see Table 1 in reference (30)]. Some *in vivo* studies seem to have found NAA to be higher in white matter (34), whereas others have found it to be higher in gray matter (27). The controversy may be resolved by more detailed study of the relaxation times of NAA in gray and white matter. Accurate relaxation times are essential for accurate metabolite concentrations [unless ultrashort  $TE$  values (1–5 ms) and long  $TR$  values (>5 s) are used], but their acquisition is time consuming, and few studies have attempted adequate measurements. NAA seems to have a longer spin-spin relaxation time ( $T_2$ ) in white than in gray matter (27), leading to overestimates of

its concentration in white versus gray matter either alone or when Cr is used as a denominator, as Cr seems to have a similar  $T_2$  in white and gray matter. NAA also has a longer  $T_1$  in gray than in white matter (34), again leading to overestimates in white matter if shorter  $TR$ s are used.

Given the neuronal localization of NAA, it is reasonable to expect it to be a marker for neuronal loss in neurodegenerative conditions; and this is exactly what is found. The association is borne out by the data for Alzheimer's disease (AD): a number of studies indicate diffuse neuronal loss in various regions in the cortex. In addition, comparisons of AD with other dementias indicate NAA loss in patients with dementia as well (35). In the case of HD, there is NAA loss in the striatum, as might be expected, but no significant loss in the cortex in the patient populations that have been examined (36,37). It might be expected that, in patients with late stage HD, there would be NAA loss in the cortex, as MRI and histopathology indicate considerable neuronal loss at this time. However, examination of these patients is complicated by their severe chorea and fragile health. Postmortem spectroscopy of tissue extracts in patients with HD revealed about 50% NAA loss in the putamen (38), and studies of HD transgenic mice showed extensive NAA loss in the striatum (39). In the case of mitochondrial encephalopathies, NAA loss is consistently found in most patients (40,41). Thus in almost every neurodegenerative condition examined to date, there is extensive NAA loss in the region of the brain affected by the pathology. This is also true in conditions such as infarcts after stroke, when NAA decreases dramatically and irreversibly (42–44).

Thus, large decreases in NAA concentration are probably the result of some neuronal loss and/or axonal damage in most pathologies. However, it should be kept in mind that, in certain conditions, NAA concentration can fall and then return to normal. This has been shown in plaques found in multiple sclerosis and demyelinating lesions (40,45,46). Furthermore, two comparisons of histopathological measurements of neuronal/glial content and NAA loss from hippocampal tissue resected for surgical treatment of temporal lobe epilepsy showed a surprising lack of correlation between NAA loss and neuronal loss (47,48). The last two results might be explained by data that we collected from transgenic HD mouse models which showed that, although there is extensive NAA loss in the striatum, it is accompanied by a decrease in neuronal area, not number (19,39). This finding was extended in two other transgenic mouse HD models in which we found excellent correlation with neuronal area, but not number (49). These findings lead to the important conclusion that decreased NAA can reflect a decline in neuronal health as well as number.

It is unfortunate that, although NAA seems to be a more or less reliable marker for neuronal loss and/or dysfunction in almost all the neurodegenerative disorders in which it has been examined, little is understood about its exact role in the brain. As most studies of neurodegeneration have assumed it to be a neuronal marker, it would be of value to understand its role in the brain, as this may shed light on the neurodegenerative process itself. NAA seems to have no role as a neurotransmitter, as it is neither excitatory nor inhibitory to other neurons. Postulated roles include involvement in lipid synthesis in myelin, both precursor and breakdown product of *N*-acetylaspartylglutamate, and as a storage form of aspartate (30). Although these roles for NAA are reasonable, they remain speculative for the most part. Some data indicate that NAA may play a role in osmoregulation (50). This study, using microdialysis, determined that hypo-osmolarity caused an increase in NAA in the extracellular space. As no other amino acids, except taurine, increased under these conditions, this increase in NAA was interpreted to be a specific response to hypo-osmolarity. Taurine has already been shown to play a role in osmoregulation, and it was reasoned that NAA may also serve this function to reduce osmotic stress and possibly prevent neuronal swelling. This hypothesis has been taken a step further with the proposal that NAA represents a 'molecular water pump' to remove the metabolic water produced during both ordinary glucose oxidation and pathological conditions (51,52). Interestingly, the enzyme that synthesizes NAA, *L*-*N*-acetylaspartyl transferase, seems to be localized in mitochondria. Thus, some of the postulated mitochondrial abnormalities in neurodegenerative disorders may also lead to changes in the concentration of NAA.

The rate of NAA synthesis and turnover has been estimated from a number of  $^{13}\text{C}$  label studies. It has been

proposed that complete label turnover of NAA is relatively slow (16–70 h) (53–55). The rate of NAA labeling is consistent in rats and humans at about 10 nmol/g/min (53,55). This relatively slow rate (compared with other energetic metabolites such as Glu) has led to the suggestion that NAA does not have a crucial role in energy regulation (53). Whatever its ultimate role in the brain, it seems fairly well established that, quantification problems notwithstanding, it will serve as a useful marker for neuronal dysfunction, and potential therapies (56), in neurodegenerative illnesses.

## Lactate

Lactate is the end product of anaerobic glycolysis. It is present in normal brain in barely detectable amounts, as evaluated by MRS ( $\approx 0.5$  mM). Therefore, when lactate is detected in measurable amounts, the result is significant. The question is significant of what? Increases in lactate can be stimulated by neuronal activation (57), and lactate can be used as a fuel by the brain (58). Lactate is postulated to play a role as a metabolic fuel by coupling Glu reuptake in glial cells after neuronal stimulation to increased glycolysis in glial cells (59). The increase in lactate concentration caused by neuronal stimulation is, however, quite small – only about a factor of two – which makes it still barely, albeit reliably, above the noise level. The amount of lactate detected in mitochondrial disorders, or in some patients with HD, is quite a bit higher than this, in some cases being fourfold to tenfold above baseline in normal controls. The amount of lactate detected by MRS represents the net balance between production and efflux and/or consumption. Therefore, it is difficult to decide whether these increases represent increased production rates or decreased rates of efflux, either through the blood–brain barrier or by reconversion to pyruvate via lactate dehydrogenase. In this regard, it is usually more important to know the lactate/pyruvate ratio because this quantity truly represents the cellular redox state through its relationship with concentrations of NADH and  $\text{NAD}^+$  (the oxidized form of NADH). Unfortunately, endogenous pyruvate concentrations are too low to be measured *in vivo* by MRS.

There are other sources of increased lactate in the brain which may not necessarily involve impaired oxidative phosphorylation. Increased macrophage activity in cerebral infarcts has been demonstrated to lead to raised lactate concentrations as a result of the high glycolytic rates of the macrophages themselves (60). Lactate concentrations were highest, and NAA and Cr concentrations lowest, in regions of high macrophage density. This type of process might be possible in late stage HD, but seems unlikely to occur in the striatum in Parkinson's disease (PD) or other slowly progressing neurodegenerative conditions. Another possible source of raised lactate concentrations is hyperventilation. It has recently

been shown that hyperventilation can induce increases in lactate concentration in normal subjects and even higher concentrations in patients with panic disorders (61). The mechanism by which this occurs is not yet clear, but, as in neuronal stimulation, lactate concentrations only increase by about a factor of two. When the mechanism by which this increase occurs is found, it may shed some light on the increases seen in the neurodegenerative disorders.

A final word about quantification of lactate is that increased lipids and macromolecules with resonances that are quite strong at 1–1.5 ppm will interfere with the lactate signal at 1.33 ppm, especially when lactate concentrations are low. In addition, use of echo times of 136 ms can often lead to gross underestimates of lactate concentration in STEAM sequences (62).

### Glutamate and aspartate

Glu and aspartate are amino acids that are excitatory neurotransmitters in the brain. The role of Glu as an excitotoxin is well documented elsewhere in a number of recent reviews (63–66) and it will not be recapitulated here. Aspartate may also function in such a role, although its concentration in the brain is about five times lower than that of Glu. Owing to their high concentrations ( $\approx 5$ –10 mM for Glu at various locations in the brain), these neurotransmitters should be easy to detect using MRS. However, one must distinguish between the metabolic pool, neurotransmitter pool, and extracellular pool of Glu. For instance, increases in extracellular Glu are likely to lead directly to excitotoxicity even though this pool is very small (much less than 1% of the intracellular pool). The intracellular pool is more closely related to metabolism than direct excitotoxic potential. In many neurodegenerative conditions, there is a decrease in Glu associated with neuronal loss. Unfortunately, detection is not easy *in vivo* at the commonly used field strength of 1.5 T. The reasons for this are the complicated spectral patterns induced by strong J-coupling at low fields and the large overlap with other metabolites, especially Gln, but including macromolecules as well. Accurate quantification of Glu and aspartate at these low field strengths is, in our opinion, nearly impossible. At 4 T, with an exceptionally good shim, it may be possible to separate Glu from Gln (67), although more routine separation is found at field strengths higher than 4 T. Almost nothing has been carried out with regards to quantification of aspartate, and this molecule will be a 'very tough nut to crack' given its large spectral overlap with the NAA methylene protons and its complicated coupling patterns.

Thus, elucidation of the role of Glu and aspartate in neurodegenerative illness using MRS awaits higher field strengths. Because Glu reuptake systems in glial cells are so potent, it may be that increases in neuronal Glu will be difficult to detect, even in cases where there may actually be transient increases. In a condition such as amyotrophic

lateral sclerosis (ALS), impaired glial uptake of Glu is found via damage to the Glu transporter excitatory amino acid transporter (EAAT2) (68,69). Thus, in ALS, increases in Glu might be postulated. This has been detected [as the sum of Glu + Gln (Glx)] using MRS in both humans in the medulla (70) and transgenic mice with mutations in superoxide dismutase 1 (71). Certainly the presence of raised Glu, as a potential neurotoxin in early HD or PD, would be amenable to testing using MRS techniques at high fields. We have detected Gln increases in transgenic HD mice, possibly as a result of impaired Glu/Gln neuronal/glial cycling (39), and a similar finding has been made in rats with quinolinic acid lesions in the striatum (an older model of HD) (72). Such a finding in humans remains to be obtained. In addition, the increases in ammonia seen in patients with hepatic encephalopathy lead to increased Gln, which is the end product of ammonia detoxification in the brain [see review in (73)].

### Choline (Cho), Cr and myo-inositol

For the sake of brevity, we have lumped these chemicals together. The peak labeled Cr at 3.03 ppm is composed of both Cr and PCr as well as smaller contributions from GABA and macromolecules. In conditions where there is impairment of energy metabolism, hydrolysis of PCr to Cr can be expected. In this case, the total resonance intensity would not change, assuming that the relaxation times were the same for both molecules. As most data indicate that the total PCr + Cr content is constant under a variety of conditions (excluding tissue necrosis or potentially cell density decrease), it is reasonable to use this chemical as a denominator in ratio methods as long as it is realized that it may not really be constant.

Cho compounds are trimethylamines which may be chemically heterogeneous. What appears to be a singlet resonance at 1.5 T often appears more complicated at higher field strengths. The Cho observed in MRS may not be entirely water soluble because *in vitro* acid extracts of brain tissue often yield smaller intensities than *in vivo* measurements (74). Also, glial cells have a 2–3-fold higher Cho concentration than neurons (33). Thus, it is possible for Cho to serve as a marker of gliosis; however, this requires histopathological correlation. It is clear that many brain tumors (as well as other tumor types) derived from glial cells are highly enriched in Cho, as rapid membrane turnover leads to a high glycerophosphocholine/phosphocholine signal (75,76), which may reflect phospholipid synthesis and breakdown rather than gliosis.

Lastly, we discuss *myo*-inositol. *myo*-Inositol is present at a much higher concentration in glial cells than in neurons (77), thus it may also be a good marker of gliosis. It also has an established role in osmoregulation, as proposed by Thurston *et al.* (78) and verified in other studies (79).

We have examined our data for the occipital cortex of 35 patients with HD and found no significant change in *myo*-inositol in this brain region compared with normal controls. The data for AD, however, seem to indicate an increase in this compound in various cortical regions. By combining this increase with the decrease in NAA, Ross and colleagues were able to distinguish AD from other dementias (35). Numerous other studies have confirmed the increase in *myo*-inositol and decrease in NAA in AD (80,81). The possible significance of this increase is not clear at this time (i.e. gliosis or osmoregulatory problems), although these authors have speculated that it may be related to changes in osmoregulation. A potential problem with measurement of *myo*-inositol is that glycine has its CH<sub>2</sub> resonance at 3.55 ppm. Although *myo*-inositol is present at an approximately 2–3-fold higher concentration than glycine, it has a shorter  $T_2$ . This should be kept in mind when analyzing purported changes in *myo*-inositol.

## QUANTIFICATION OF <sup>1</sup>H MRS

Quantification of <sup>1</sup>H MRS has been slowly evolving over the years because of the many difficulties in ‘absolute quantification’. The problem can be largely attributed to difficulties in determining accurate relaxation times or avoiding macromolecular contamination. Often the denominator is chosen to be the Cr/PCr peak at 3.0 ppm because of its supposed insensitivity to the state of the tissue. It has also become common practice to report ‘absolute’ concentrations using water as an internal standard because of its relative molar invariance. This practice is also fraught with some difficulty, especially in neurodegenerative diseases. As much brain tissue in older subjects and patients with neurodegenerative diseases will be somewhat atrophied, the possibility of cerebrospinal fluid (CSF) contamination is high. As CSF has spin-lattice relaxation time ( $T_1$ ) and  $T_2$  properties quite different from tissue water and neurochemicals, the degree to which it contaminates the voxel must be known. Further, metabolite relaxation times can vary between white and gray matter (27,34), which means that how much each of the large spectroscopic voxels is composed of white and gray matter must be known. This problem is more severe in humans than in mice because of the lissencephalic brain of the mouse. In addition, because of the large overlap of metabolites with tissue macromolecules, the unique determination of  $T_1$  and  $T_2$  for each neurochemical is quite difficult, as the macromolecular contamination is much higher at the shorter  $TE$ s. Going to higher magnetic field strength helps in this regard, as there are now more Hz per ppm, but even at 9.4 T there is substantial macromolecular intensity under the NAA, Glu/Gln and Cr resonances (82).

A brief, but general, discussion of the quantification problem is given below. To convert the observed

resonance intensity at a given frequency (here chosen to be NAA at 2.0 ppm) into a concentration using water (at 4.7 ppm) as an internal standard, we arrive at an equation that looks something like the following (for a simple spin echo sequence):

$$[2.0 \text{ ppm}] = \frac{A(2.0 \text{ ppm})}{A(4.7 \text{ ppm})} 80M$$

$$\frac{A(2.0 \text{ ppm})}{A(4.7 \text{ ppm})} = \frac{\sum_{i=1}^n M_0^i [(1 - \exp(TR/T_1^i)) \exp(TR/T_2^i)]}{\sum_{j=1}^n M_0^j [(1 - \exp(TR/T_1^j)) \exp(TR/T_2^j)]}$$

where  $A$  (ppm) is the area at a given frequency,  $M_0^i$  is the magnetization of the  $i$ th resonance at that frequency (necessary because so many neurochemical resonances overlap, such as NAA and Glu at 2.0 ppm), and likewise the  $T_1^i$  and  $T_2^i$  are the longitudinal and transverse relaxation times of the  $i$ th components,  $M_0^j$  is the water magnetization of the  $j$ th compartment, with its longitudinal ( $T_1$ ) and transverse ( $T_2$ ) relaxation times (necessary because a given voxel may contain white matter, gray matter, and CSF in different amounts and these all have different relaxation times), and we have assumed that the molar proton concentration of water in the brain is  $\approx 80$  M. It is apparent that this is a tricky problem, notwithstanding the fact that a further complication relating to the splitting of resonances by ‘J-coupling’ is ignored in the equation above.

A common approach to quantification fits linear combinations of metabolite sub-spectra to the observed spectra [the LC model approach (83)]. This is an eminently reasonable approach and incorporates constraints into intensities by fitting all the peaks of a given molecule together. It should be noted that this can lead to decreased accuracy when either or both of two likely conditions apply. The first is if different resonances have different effective  $T_2$  values. This is probably the case for NAA, where the methyl peak at 2.0 ppm has a much longer  $T_2$  than the methylene at 2.62 ppm. The second is, if the radio frequency pulse profile is not uniform across the spectral width, this can adversely affect the intensities. This problem is somewhat averted by using the metabolite basis spectra acquired on the same scanner, but can be significantly affected by subject motion (unpublished observations). Any method will suffer from the problem that the relaxation times for both metabolites and water go undetermined (indeed they have to for a reasonable total acquisition time) and the macromolecule contributions are undetermined except as baseline noise or as basis sets from healthy controls. The obvious solution to this problem is to collect with as short an echo time as is possible (down to  $< 3$  ms) thereby minimizing the contribution of  $T_2$  to the uncertainty. This is, of course, quite useful; however, it also introduces the problem of macromolecules. It has been shown that, without

incorporation of prior knowledge of the macromolecules, it is impossible to obtain concentrations of metabolites consistent with the biochemical literature (84). The macromolecular components are largely undetermined biochemically, and it is not known how they may change in disease. Thus they may prove very difficult to remove using a priori information from 'template' spectra of controls. It is apparent that this is a major problem, and most 'absolute' quantifications reported in the literature should be taken with a grain of salt. That this is true can be seen from 'absolute' determinations of NAA concentration in human cortex by MRS ranging from 7 to 11 mM in the literature. Further, the macromolecular resonances yield large signal intensity under the Glx peak as well as, to a lesser extent, the Cr peak at 3.0 ppm. Therefore, if one uses very short echo times, it becomes paramount to have excellent lipid suppression in place. Collection of metabolite nulled spectra and macromolecule nulled spectra using a preceding inversion pulse can be extremely helpful in this regard for identification of the macromolecular profile (82). The macromolecular resonances have been histologically associated with microglial infiltration in stroke patients (85), potentially turning them into useful markers for that important process.

If one wishes to merely compare control populations with neurodegenerative populations or patient populations longitudinally, then, as long as one uses consistent methods, useful and statistically significant data can be obtained. Often this problem is dealt with by taking ratios of peaks rather than absolute concentrations. Usually the Cr peak at 3.0 ppm is used as the denominator because of its relative invariance in multiple pathologies compared with the other major peaks. When comparing the ratios, it is important to note that, because of the complexity of the equations above, the ratios will probably change at different  $TE$  values. Thus, the NAA/Cr ratio, for instance, is greater at  $TE = 272$  ms than at 136 ms. This means that direct conversion of a decrease in NAA/Cr ratios into percentage neuronal loss is dangerous.

## SPECTROSCOPY IN MICE – HARDER THAN IN RATS!

The increasing use of higher magnetic fields allows increased SNR (and consequently smaller voxels) as well as increased spectral dispersion in MRS. This means that in areas of the brain where the magnetic field is quite uniform, such as the thalamus or striatum, beautiful spectra can be obtained [see for instance (25,72)]. Unfortunately, the increased magnetic field can also make the collection of high-quality spectra in mice more problematic than in larger animals such as rats or humans. The small size of the mouse raises two challenging problems. The first is the air/tissue interface leading to large gradients as a result of the large differences in

magnetic susceptibility between the air and the tissue. As the mouse head is smaller than, for instance, the rat head, the brain is closer to the air and the air/tissue susceptibility interface can lead to difficulty in shimming (the act of making the magnetic field more homogeneous using auxiliary gradient coils) the superficial cortex. As with humans, areas near sinuses suffer from worse line broadening at higher fields than at lower fields. In rodents, at high field, it is quite difficult to obtain high-quality spectra in areas such as the amygdala and inferior temporal cortex. Yet another problem presents itself as the result of the small size of the mouse. The air-filled lungs are much closer to the brain than they are for a rat, and the movement of the lungs during breathing leads to periodic oscillations in the  $B_0$  field. As a mouse breathes at about 100–200 breaths per minute (1.7–3.3 Hz), there may be line broadening that may potentially be corrected for by respiratory gating and binning of the data, although to our knowledge this has not been attempted in mice yet. As noted, it is possible to collect individual spectra during the acquisition. In this way, each of the spectra can be individually corrected for frequency shifts and eddy current effects (if the water spectrum is obtained), even in the absence of gating, and this can improve the overall spectral quality (86). Obviously, with the exception of the breathing, these issues become more or less problematic depending on which brain region one wishes to investigate. If one makes a  $B_0$  field map of the mouse brain (or even a  $T_2^*$  histogram), it is quite clear that the  $B_0$  varies in a predictable manner.

Other than the problems noted above, MRS in mice presents the same problems as for other species, including quantification, often unmeasured relaxation times, water and lipid suppression. Owing to the small sizes involved, it places more of a burden on eddy current performance of the gradients (because of the increased gradient strengths necessary for selection of the smaller voxels), but this presents few problems with modern spectrometers and can, in principle, partially be corrected for by simultaneous (interleaved) collection of unsuppressed water spectra. There are two other problems when scanning mice. The first is the fact that mice are very sensitive to temperature fluctuation, so body temperature must be controlled more carefully than is necessary with larger animals. The second is, owing to the small respiratory capacity (or tidal volume) of the mouse, more care must be taken than for larger animals to construct masks that avoid rebreathing in animals that receive gaseous anesthesia. The small sizes mean that spectroscopic imaging is more challenging because of the smaller voxel sizes and the requisite SNR constraints. On the other hand, signal averaging for periods of time up to hours is not problematic in most situations.

Another very important issue to be considered in MRS studies of transgenic mice is the potential variability of metabolite concentrations in different strains of mice. An older study of NAA concentrations in a variety of different mouse strains showed that they varied by up to

almost a factor of two between various strains (87). It is very much the case that different strains of mice are used to generate the transgenic neurodegenerative models. Thus, it is imperative to control for background strain when comparing a transgenic animal with a wild-type animal as a control. A more important question is why are NAA concentrations so variable between strains? In this regard, the value of correct tissue handling *post mortem* for *in vitro* neurochemical analysis cannot be overestimated. Smaller tissue specimens degrade faster than larger ones as the result of thermal equilibration. One problem in analysis of *in vitro* spectra, whether from brain extracts or from intact tissue samples using high-resolution magic angle spinning (HRMAS), is that the tissue must be processed and frozen quickly, otherwise significant degradation can take place. This degradation will involve loss of NAA and concomitant increases in acetate (88). Lactate will also show large increases compared with tissue that is processed more quickly. Presumably, if wild-type and transgenic mice are handled in a similar manner, the results will be comparable.

We compared a number of different mouse models in a recent paper (49). There was little variation in the NAA concentrations of wild-type mice of different strain,

reinforcing, to some degree, the value of *in vivo* spectroscopy, which is largely immune from questions of sample handling.

### $^{13}\text{C}$ NMR SPECTROSCOPY

Although carbon is less sensitive than even phosphorus (the relative sensitivities of proton/phosphorus/carbon is 100:6.7:0.018), it is a useful marker for a number of interesting biological pathways. Advances in indirect detection of  $^{13}\text{C}$  through coupling to protons has greatly increased the potential sensitivity (89–91). Further gains in sensitivity have been attained using hyperpolarized  $^{13}\text{C}$  (92,93), although the hyperpolarization decays rather quickly as a result of  $T_1$ . Because the natural abundance of  $^{13}\text{C}$  (the MRS active isotope with spin 1/2) is only 1.1%, molecules can be labeled and seen as they are metabolized. Such studies can be performed using glucose as a label to be followed as it passes through the TCA cycle. Usually the C1 position of glucose is labeled using  $^{13}\text{C}$ , then the metabolism of the glucose molecule through the glycolytic pathway and then the TCA cycle is followed. A schematic for this is shown in Fig. 3. On the first passage through the TCA cycle, the

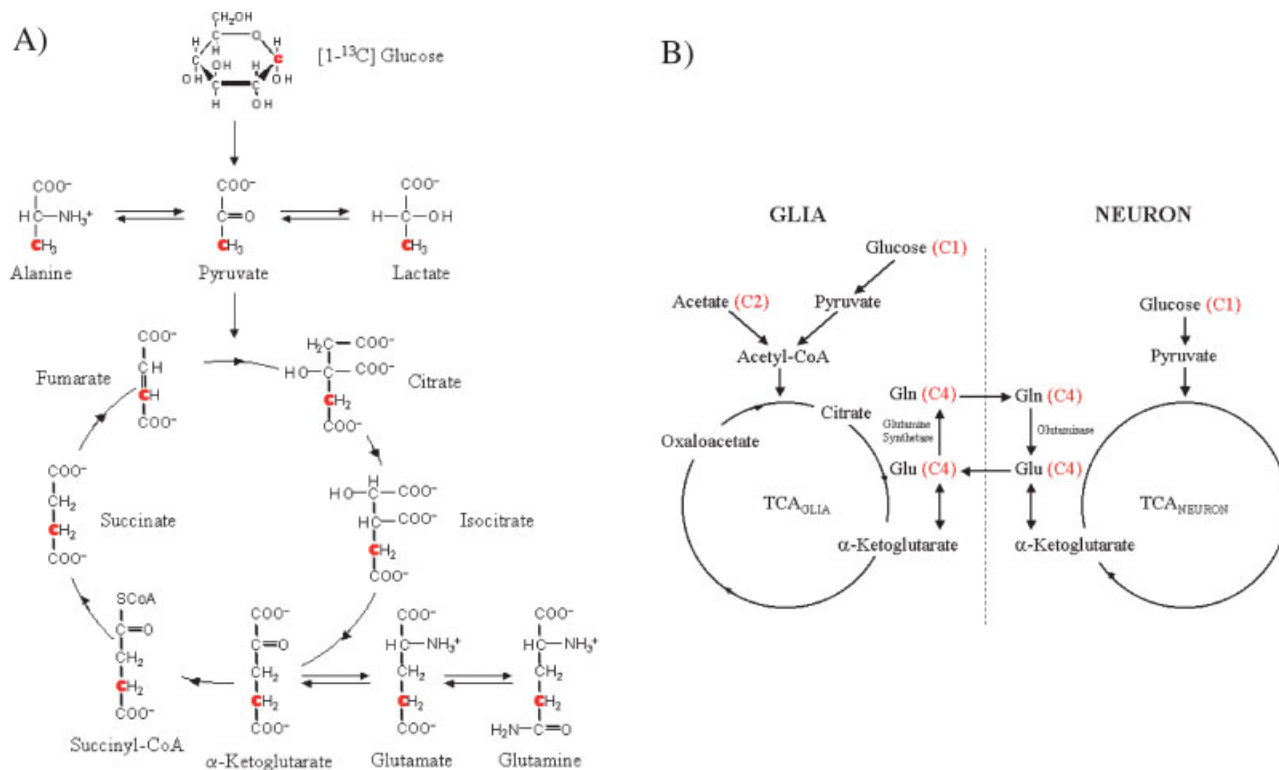


**Figure 3.** (A) Schematic for the metabolism of glucose and its conversion into observable  $^{13}\text{C}$ -labeled compounds. The Cs in bold represent the carbon as it passes through the TCA cycle. Note that, on the first passage, the Glu and Gln are labeled at the C4 position. If the TCA cycle is blocked by, for instance, 3-nitropropionic acid, an increase in lactate and alanine is seen, as well as a build up of succinate. (B) Schematic of neuronal/glial metabolism and Glu/Gln cycle. Neurotransmitter release of Glu is taken up by the astrocyte where it is converted into Gln and shuttled back to the neuron, where it is reconverted into Glu. Also shown is the metabolism of acetate, which is only taken up by glial cells, and hence can provide a means to discriminate neuronal from glial metabolism using  $^{13}\text{C}$  MRS.

primary detectable molecule is  $^{13}\text{C}$ -labeled Glu in the C4 position, followed quickly by Gln at the C4 position. Subsequent passages through the TCA cycle produce labeling at the C3 and C2 positions of Glu and Gln. The absolute amount of  $^{13}\text{C}$ -labeled glucose in the brain can also be detected at the same time. At later time points, other metabolites, such as lactate, GABA and NAA, start to appear.

In addition to glucose, acetate can also be labeled. This provides an interesting comparison with glucose labeling, as acetate is only taken up by glial cells and can be used to probe altered glial metabolism as shown in Fig. 3(94–97).

Much work has gone into modeling the kinetics of the reactions and determining, for instance, TCA cycle flux and Glu–Gln cycling from these numbers. Space precludes a full discussion here; however, most researchers who study brain make the assumption that the reaction from oxoglutarate to Glu is much faster than the rate at which the substrate enters (i.e. TCA cycle flux), therefore the rate of C4 labeling is essentially the rate of TCA cycle flux. Although this approach is somewhat controversial, its validity does not affect our qualitative understanding here. The rate at which the various TCA cycle intermediates become labeled yields the desired information in the context of a metabolic model (98–102). Thus, administration of  $^{13}\text{C}$ -labeled glucose would yield a lower rate of labeling of Glu in a patient with a suspected defect in glycolysis than in a control subject. At this point, such an observation would be indistinguishable from a defect in the TCA cycle. Preliminary data have been obtained for AD: Glu labeling correlated with both reduced NAA (and NAA/*myo*-inositol) and measures of cognitive impairment (103). Large increases in lactate labeling and decreased Glu and NAA labeling were found in  $^{13}\text{C}$  spectra in two patients with mitochondrial disorders (95). We have shown increased Glu metabolism in mouse models of ALS, and decreased Glu and increased Gln labeling in an HD mouse model (104). These results are consistent with impaired neurons in HD and impaired glial function in ALS.

$^{13}\text{C}$  NMR has also proved useful for investigating rates of synthesis of molecules such as NAA and glutathione in the brain. A number of studies have examined NAA turnover either using  $^{13}\text{C}$ -labeled glucose infusion or by feeding an animal a  $^{13}\text{C}$ -enriched 'chow' (54). The results all agree that complete NAA turnover is quite slow, of the order of days (53,54,105).

Although the biochemical specificity of  $^{13}\text{C}$  MRS is tantalizing in its potential, it is unlikely to be used as extensively as  $^1\text{H}$  MRS because the cost of  $^{13}\text{C}$ -labeled glucose and the limited spatial (and temporal) resolution obtainable are likely to limit widespread application to humans. Nonetheless, it remains a very useful tool for investigating etiological and symptomatic questions in neurodegenerative illness, especially when combined with  $^1\text{H}$  MRS and other techniques such as positron emission tomography (PET).

## USE OF MRS IN STUDIES OF THERAPEUTICS IN HUMANS

The use of MRS to study neuroprotection can only be defined as being in its infancy for any number of reasons that are not worth digressing into here. Suffice it to say that, at this point, as the end point in any human therapeutic trial, MRS can only be considered as complementary to other end points including clinical metrics. On the other hand, there are numerous animal studies in which MRS data can be considered a major criterion for evaluation of the animal's neurochemistry. Instead of cataloguing the various studies that have been performed, let us examine what major end points may prove useful in future studies.

Because NAA is typically the largest peak in the MR spectrum, it remains an attractive target for assessment of therapeutic interventions. There are two reasons for this. First, in any trial, reproducibility from one time point to the next is important. Owing to the low sensitivity of MRS as well as the relatively low concentrations of neurochemicals such as NAA, it is imperative to maximize intra-subject reliability. This is best attained using resonances with the highest SNRs. This is a useful, but hardly compelling, reason. Secondly, as NAA is a marker for the health of neurons, it can be imagined to be a therapeutic marker in any pathology in which the loss of neurons is expected, such as AD, HD and ALS. As neuronal loss in these pathologies proceeds fairly rapidly, NAA is a reasonable choice for following neuronal loss. Among the complications that make such a study difficult is the need for reproducibility of the voxels (whether they are acquired as single voxels or as multiple voxels from a spectroscopic image). Because gray and white matter have different amounts of NAA, it is important to collect a high-resolution three-dimensional MR image to assess the amount of gray and white matter in each voxel as well as to correctly register the voxels (34).

A number of studies have used NAA as a therapeutic marker in humans. A study of epilepsy showed re-normalization of NAA in patients rendered seizure-free after surgery (this re-normalization was significant compared with both before surgery and patients who were not rendered seizure-free) (106). NAA has also been used as a marker for recovery in treatment of ALS with riluzole (56,107). In this case, a small increase in NAA concentration (6%) was recorded in the motor cortex in patients treated with riluzole. The untreated group showed a decrease in NAA of about 4%. Studies of other more affected brain regions, such as the medulla where NAA is decreased by 17% compared with controls (70), may provide better sensitivity. Furthermore, large increases in NAA/Cr ratios were found to correlate with improved recovery from traumatic head injury (108).

An intriguing use of MRS has been proposed for following the results of treatment for PD in both primate models (109) and human patients (110) after grafting of

dopaminergic fetal cells into the striatum. As fetal cells possess very little NAA, it is possible to measure changes in NAA concentration longitudinally after grafting. Presumably increases in NAA concentration would indicate that the graft is surviving and generating axonal sprouting (110). Evaluation of NAA concentration may prove complementary in this regard in the study of dopamine transporter concentrations and binding using PET.

Use of NAA could thus be a powerful adjunct to other techniques for assessing neuroprotective strategies such as *N*-methyl-D-aspartate antagonists in stroke, anti-epileptic drugs, and potential treatments for ALS, AD, and HD. Indeed, any neurodegenerative condition in which progression of symptoms is rapid enough to assess neuroprotection in a reasonable time window could be studied. One important issue that must be settled in such a study is that of neuronal loss versus neuronal health. In the former case, one would expect to find a slower rate of NAA loss than in untreated controls, whereas in the latter one may actually see an increase in NAA concentration if the neurons have not actually died.

## NEUROPROTECTION IN ANIMAL MODELS

The non-invasive nature of MR makes studies of neuroprotection attractive. The ability to follow an animal longitudinally, and as its own control, allows evaluation of neuroprotection with smaller numbers of animals than might be required for histological methods. These types of MRS experiment have been performed in many of the transgenic mouse models. In addition, many of the principles have been demonstrated in toxin models of neurodegeneration. Many, but not all, of the toxin models have been supplanted by the transgenic models. For instance, although HD, AD, and ALS pre-clinical therapeutic studies have now migrated to the excellent transgenic animal models discussed below, PD is largely still modeled using the toxin, 1-methyl-4-phenyl-1,2,3,6-tetrahydropyridine (MPTP), as it faithfully replicates a wide spectrum of the PD pathology. Examples of the neuroprotective strategies evaluated using MR techniques include:

- (a) Glu blockade by either antagonists such as MK-801 or ablation of the cortical input of Glu into the striatum via decortectomy (15,111–115);
- (b) blockade of free-radical production using blockers of neuronal nitric oxide synthase or trapping of free radicals after they are formed with compounds such as *n*-*t*-butyl- $\alpha$ -(2-sulfophenyl)nitron (116,117);
- (c) administration of neuronal growth factors such as basic fibroblast growth factor (118);
- (d) energy repletion strategies whereby attempts are made to restore ATP concentrations with, for instance, mitochondrial electron transport chain substrates (e.g.

coenzyme Q<sub>10</sub> or ubiquinone) or Cr supplementation (13,18,19,71,119,120).

Many of these strategies have proved useful in models of focal ischemia.

MRS may have a role in assessing the efficacy of such potential therapies by monitoring their effects on: neuronal health and number using NAA; oxidative phosphorylation using lactate or ATP; lesion size as measured by water imaging.

NAA has been shown to be a useful marker for neuroprotection against MPP<sup>+</sup> lesions using neuronal growth factors (118). In this study, basic fibroblast growth factor was found to protect against neuronal loss, as measured by spectroscopic imaging of NAA determining absolute NAA relative to water from proton density-weighted images (i.e. images in which *TR* is long and *TE* is short and in which CSF, edema and brain are nearly iso-intense) in the same animals. It is important to note that all the neurochemicals from one spectrum can be measured, and thus neurodegeneration can be analyzed from a number of different perspectives with regard to neuronal loss and energy metabolism.

Numerous other animal studies have used NAA as a marker for neuroprotective strategies. Our own studies have used NAA as a marker for neuroprotection in both neurotoxin models of neurodegenerative illness using blockade of mitochondrial complex II (succinate dehydrogenase) (120) or complex I (MPP<sup>+</sup>) (118), as well as in transgenic mouse models of HD (19). In the latter study, it was found that dietary Cr supplementation (2% Cr in the food) leads to an increase in lifespan of R6/2 mice from about 15 weeks to about 17.5 weeks. Cr supplementation also leads to a 30% increase in NAA in the striatum of these mice. These mice typically suffer loss of more than 50% of NAA in the striatum (39). MRS can simultaneously measure the Cr increase in the brain and NAA and other neurochemicals by using, for instance, water as an internal reference standard. Thus, in the latter study, we showed an increase in brain Cr concentration of 21%. Most importantly, the increase in NAA concentration correlated with the increase in Cr concentration. Protection of the NAA concentration also correlated with protection of neuronal size (about 31%) by Cr supplementation. As NAA has an exclusively neuronal localization, the decrease in neuronal size leads to a decrease in the total NAA signal detected. These results show that the time course of neuronal shrinkage is roughly parallel to that of NAA loss in the absence of Cr treatment. Cr supplementation delays both the loss of NAA and neuronal shrinkage to approximately the same degree. These again reflect the utility of NAA as a neuronal marker.

We also studied the ability of Cr to neuroprotect in a transgenic mouse model of ALS using a mutation in superoxide dismutase. The lifespan of these mice was prolonged by about 20% with 2% oral Cr supplementation (18). Further, the Cr lowered the raised Glu

concentrations as measured by  $^1\text{H}$  MRS. The peak labeled Glx is smaller in the mouse with ALS after Cr supplementation at about 80 days of age. Unfortunately, the effect wears off at 120 days, at which time the raised Glx reappears in spite of Cr supplementation (18).

## ALZHEIMER'S DISEASE MOUSE MODELS

A number of different mouse models of AD have been developed based on genes associated with human familial AD [reviewed in (121)]. The first model developed was the amyloid precursor protein (APP) model based on known familial mutations in this gene. This is known as the Tg2576 model, which overexpresses a human APP cDNA transgene with the K670M/N671L double mutation (APP<sub>swe</sub> or Swedish mutation from the location of the family where the gene was originally identified). This model develops plaques starting at about 6 months of age and shows memory deficits when tested on a water maze. The plaque distribution is primarily in the cortex and hippocampus, and, at later ages, is quite pronounced in the cingulate cortex. Our group studied this model using both *in vivo* spectra at 4.7 T and *in vitro* spectra. The data show that at 18–20 months of age, there was decreased NAA and Glu and increased taurine compared with the wild-type controls (122). Using the *in vitro* spectra, we were also able to show a decrease in GSH. Interestingly,

*myo*-inositol, a compound that is often raised in AD brain, was not increased in this model. These findings were confirmed in a subsequent study of these mice (86). The latter study also examined the age-dependent spectroscopic changes noted in another mouse model of AD, the so-called APP  $\times$  PS1 (presenilin 1) model. The APP  $\times$  PS1 model starts to develop plaques at an earlier age than the single transgene APP mice. In the APP  $\times$  PS1 model, there was an age-dependent increase in *myo*-inositol and decreases in NAA and Glu. The changes in *myo*-inositol were only significant after about 400 days of age. Figure 1 from the Marjanska *et al.* paper (86) showing the age-related changes is reproduced here as Fig. 4. Both these models showed decreased NAA and Glu. Whereas the APP  $\times$  PS1 mice showed increased *myo*-inositol, the APP mice showed increased taurine. Interestingly, both *myo*-inositol and taurine have postulated roles as brain osmolytes, as mentioned above. Why there should be this difference between these two models is not known. In patients with AD, there is an increase in *myo*-inositol; however, as humans have little taurine in the brain, it is unlikely that there would be increased taurine in the AD brain.

A third MRS study examined yet another model of AD using the same APP mutation but a different PS mutation referred to as PS2 (123). These mice developed plaques at a later age than the APP  $\times$  PS1 mice. The APP  $\times$  PS2 mice showed a similar age-dependent decrease in NAA

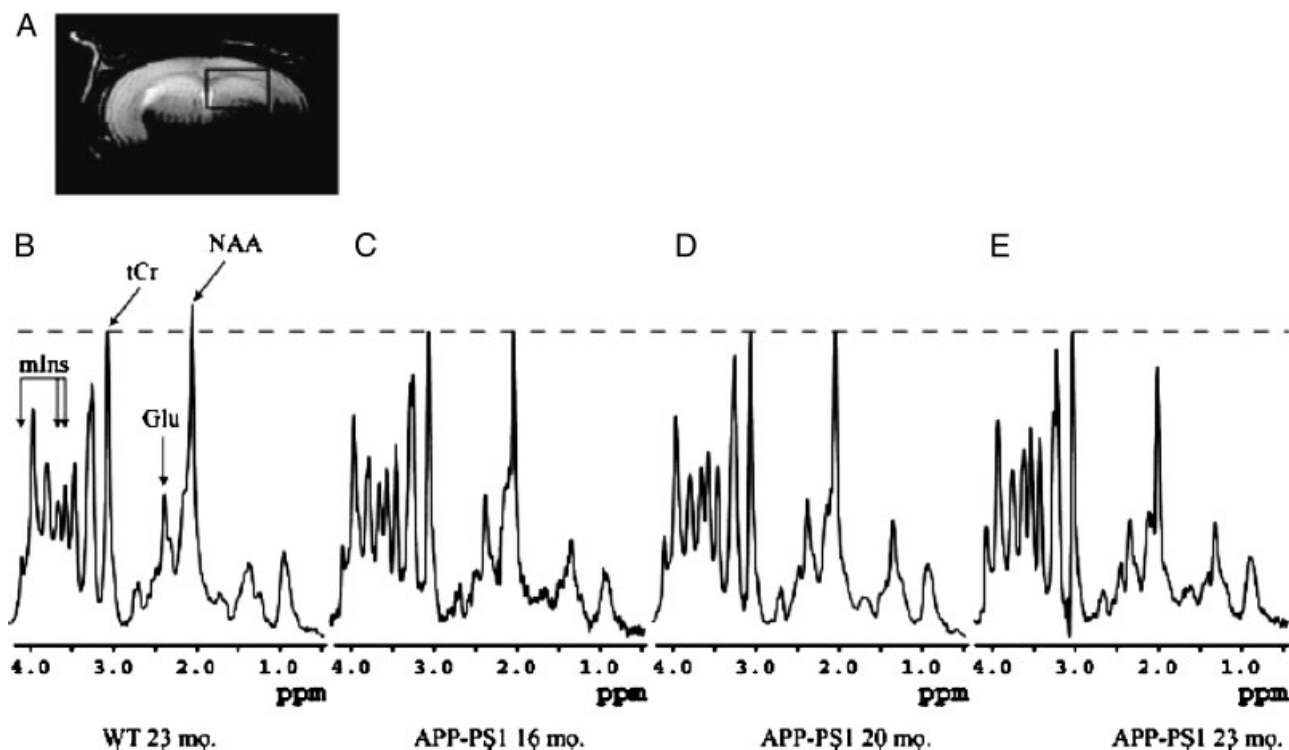


**Figure 4.** Age-related changes in metabolites in APP  $\times$  PS1 mice at 9.4 T. Representative image and spectra of mouse brain. (A) An image of mouse brain with placement and size of the voxel. (B–E) Localized *in vivo*  $^1\text{H}$  NMR spectra obtained from 18  $\mu\text{L}$  voxel (box in A) from the brain of a 23-month-old B6 SJL wild-type (WT) mouse (B) and an APP  $\times$  PS1 mouse scanned at 16 (C), 20 (D), and 23 (E) months of age. The spectra are shown with similar linewidths and with amplitude adjusted by using the total Cr (tCr) peak at 3.03 ppm. Reproduced, with permission of authors and publisher, from (86).

and Glu that correlated with the plaque burden in the 24-month-old animals. No spectroscopic abnormalities were found before 16 months of age. Interestingly, in this model there was no increase in *myo*-inositol, similar to the APP model. These authors also found increased ventricular size in the animals with AD, but no gross brain atrophy like that seen in patients with AD.

We have been studying yet a third model of AD, so-called triple-transgenic animals, with mutations in APP  $\times$  PS1 as well as a tau mutation to generate the neurofibrillary tangles found in humans, but lacking in the other mouse models (124). We have used both *in vivo* and *in vitro* spectra using HRMAS. Data from the hippocampus are shown in Fig. 5. At 6 months of age, there is already a decline in NAA in these mice.

As NAA decreases and *myo*-inositol increases, the ratio of these two has been proposed as a more sensitive spectroscopic marker for following the human disease (35). This would appear to be true also in mouse models such as the APP  $\times$  PS1. However, one should be cautious in the use of such ratios. One reason is that, if NAA

and *myo*-inositol represent two different pathological mechanisms and tissue/cellular compartments, they may show independent temporal profiles as the disease progresses and the ratio may mask this. For instance, in the study of APP  $\times$  PS1 mice (86), NAA appears to decline fairly linearly with age, whereas the *myo*-inositol does not show an increase until after 400 days of age. This fact may reflect the different roles and cellular compartments of NAA and *myo*-inositol, the former being primarily neuronal and the latter glial.

One trend in the use of MR techniques is greater use of the multifarious MR parameters that are measurable (125). Therefore, once a mouse is placed in the magnet, there is great incentive to collect other data besides MRS. A number of interesting studies of AD mice have appeared. Jack and colleagues (126) showed that one could image plaques in APP  $\times$  PS1 mice using MRI microscopy of *ex vivo* brains. The plaques generate  $T_2^*$  contrast with surrounding tissue as a result of the large iron accumulation in the plaques. These results were extended to *in vivo* studies (with the concomitant decrease in spatial resolution), and there was some evidence that, at later ages, increased  $T_2/T_2^*$  contrast attributable to plaques could be detected (126). The use of spin echo images allowed detection of the plaque geometry, whereas gradient echo MRI allowed detection of plaque iron content. As field strengths continue to increase, thereby increasing SNR and susceptibility contrast, it should become more attractive to combine such studies for both animal and human systems with MRS studies. Other authors have examined hemodynamic parameters in APP mice, showing decreases in cerebral blood volume at 4 months in the cortex, hippocampus and thalamus (127). Such studies are relatively quick to perform and may greatly add to the total information obtained from the MR examination. These data should allow more comprehensive comparisons with histological and molecular information.

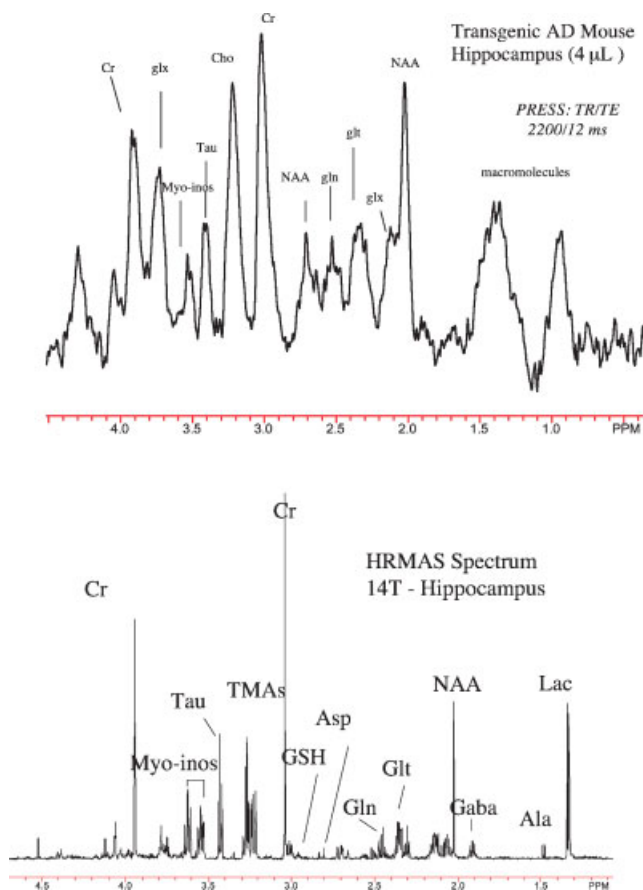


**Figure 5.** Spectra from the hippocampus of 3  $\times$  Tg AD mice. Top, Spectrum from the hippocampus (4  $\mu$ L) at 9.4 T using a PRESS sequence (TR/TE 2200/12 ms). Bottom, Piece of hippocampal tissue ( $\approx$ 2  $\mu$ L) scanned at 14 T using HRMAS after  $T_2$  filtering with a CPMG sequence. The spectrum is similar to, although not as rich as, *in vitro* brain extract spectra. The spectra show decreased NAA compared with the wild-type.

## HUNTINGTON'S DISEASE MODELS: EFFECTS OF GENE CONSTRUCTS, GENE MUTATIONS, GENE EXPRESSION AND GENE CONTEXT

HD is a relatively rare neurodegenerative disorder that is part of a family of neurodegenerative disorders called triplet repeat diseases. In the case of HD, the mutation turned out to be in a previously unknown gene coding for a 364 kDa protein now called huntingtin (htt), the function of which is still unknown. In normal controls, the triplet repeat (CAG)<sub>n</sub> varies from 6 to 35. Most HD sufferers have 40–45 repeats. The triplet codes for polyglutamine, and it is known that when the gene is cleaved, to give polyglutamine oligopeptides, it is much more toxic. Human MRS data show decreased NAA (36,128,129). Small increases in lactate have also been noted in this

disease (36,130). The decreases in NAA correlate with CAG repeat length in patients in a manner similar to neuronal loss (37).

A number of different transgenic mouse models have been created with various numbers of CAG repeats. One of the first strains created was the R6/2 mouse. These mice express an N-terminal fragment (exon I only) of the human HD gene with 150 CAG repeats and develop a progressive neurological disorder with features similar to juvenile-onset HD (131). At 6 weeks of age, R6/2 mice show loss of body and brain weight, at 9–11 weeks they develop abnormal motor function and epileptic seizures, and they die at around 100 days of age (131). The brains show striatal neuronal atrophy, without much neuronal cell loss, and intranuclear inclusions that are immunopositive for htt and ubiquitin (19,132). Another strain of mice referred to as N171-82Q express a cDNA encoding a 171-amino acid N-terminal fragment of htt containing 82 CAG repeats (133). The findings for these mice are similar to those obtained for the R6/2 mice, but they have a more delayed disease onset and longer survival, with the phenotype beginning at about 90 days of age and death at around 135 days of age (18,133). These mice also show selective striatal pathology, unlike the R6/2 mice in which the striatum and cortex are equally affected. Hayden and coworkers (134) produced yeast artificial chromosome (YAC) transgenic mice expressing mutant htt with 72 CAG repeats (YAC72). Two strains of these mice were developed, one with a relatively normal expression level of htt (line 2498) and another with a low expression level of htt (line 2511). Mice of the 2498 line have a similar disease phenotype to the R6/2 and N171-82Q

mouse models above, but an even later onset, with electrophysiological abnormalities from 6 months of age and striatal neurodegeneration appearing at 12 months of age (134). Mice of the 2511 strain have milder symptoms still and a very mild phenotype. The use of these mice allows comparison of the effects of expression levels as well as CAG repeat length. In addition, to study the effects of gene context, we also studied a model in which an expanded CAG repeat is introduced into the mouse hypoxanthine phosphoribosyltransferase (HPRT) gene (2). These mice develop motor abnormalities and nuclear inclusions similar to the other mice, but also have many different phenotypic characteristics, such as weight gain.

van Dellen *et al.* (135) characterized R6/1 mice. These mice have only exon I of the human htt gene with 111–121 CAG repeats. They typically show an onset of symptoms at approximately 4–5 months of age. At this age they have no overt neuronal loss, although there is a small decrease in striatal volume. There is also a 26 % decrease in NAA. We examined R6/2 mice, which also have the same exon I of human htt but have about 150 CAG repeats. We used *in vivo* and *in vitro* spectroscopy and compared the strain with the other strains noted above (39,49). Figure 6 shows spectra from the striatum comparing an HD mouse with 141 CAG repeats with a wild-type mouse. Also shown are spectra from a wild-type and HD mouse brain extract. There is extensive loss of NAA, and increases in taurine, Cho and Gln are detectable *in vivo*. Owing to overlap of the taurine triplet at 3.27 ppm with the Cho resonance at 3.23 ppm, it is possible that some or all of the Cho increase is due to the increase in taurine. In the *in vitro* spectra, the greatly

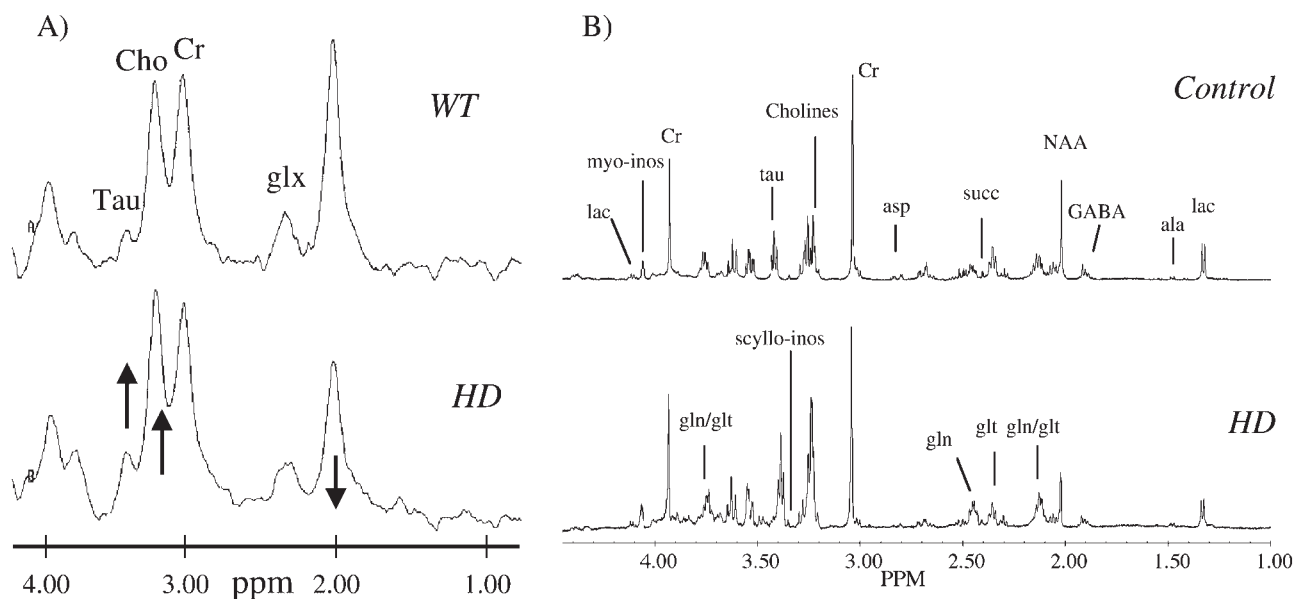


**Figure 6.** (A) Typical <sup>1</sup>H spectrum from striata in a wild-type mouse (WT) and a transgenic HD mouse with 141 CAG repeats (*TR/TE* 2000/136 ms; 4.7 T). Note the increases in taurine (Tau) and Cho and the decrease in NAA. (B) Comparison of <sup>1</sup>H spectra from striatal extracts of a wild-type and the same HD mouse model as in (A). The greatly increased spectral resolution and sensitivity allows many more resonances to be quantified. The same pattern is detected as is found *in vivo*. Spectra were acquired at 500 MHz.

increased spectral resolution and sensitivity demonstrate changes in other peaks such as increases in *scyllo*-inositol. The data we collected showed decreases in NAA, Glu, and succinate, and increases in Gln, taurine, *scyllo*-inositol, but not *myo*-inositol, and glucose. Interestingly, we discovered a huge increase in glucose in R6/2 mice using MRS. This led us to discover that they had diabetes at the later stages, a fact we, and others, later confirmed using other techniques and tools. This provides a good example of how MRS can be used to make a completely novel ancillary biological finding.

The decrease in NAA was exponential from the onset of symptoms to death. We confirmed this relationship in a later study with even more mice showing that the NAA decline matched the functional form of the decline, not in neuronal number, but neuronal area (49). Thus, the neurons shrink, but can still be measured. This shrinkage in neuronal area may well explain why an increase in taurine is noted in these mice, as it has been implicated in regulation of brain volume (136).

The decline in NAA over time fits well to the following exponential function:

$$\text{NAA}(\text{obs}) = \text{NAA}(\text{d}) + [\text{NAA}(\text{p}) - \text{NAA}(\text{d})] \\ \times \exp[-(\text{age} - \text{AO})/\text{NAA}(\text{t})]$$

where NAA(d) is the NAA concentration at death, NAA(p) is the pre-symptomatic concentration (equal to the wild-type concentration), and AO is the age of onset. This same exponential-like loss was seen in the neuronal area. Interestingly, the increases in taurine and Cho were apparently linear with age in the R6/2 mice. In the same

study, we examined a number of other HD mouse models developed to examine various aspects of the gene mutation (49). These models explored the effects of CAG repeat length (18 vs 82 CAG repeats), gene expression levels, and even the effects of expanding a CAG repeat on a completely different gene (HPRT mice). One of the more striking findings is that reducing the CAG repeat length leads to a much less severe phenotype, with NAA loss only in the striatum and not in the cortex. Further, these mice showed a linear decrease in NAA rather than an exponential loss as noted in the R6/2 mice. Similar to the R6/2 mice, there was also excellent correlation in these mice of NAA loss with neuronal shrinkage, rather than frank neuronal loss (49). These effects are shown in Fig. 7.

R6/2 mice also show large increases in Gln. The separation of Glu from Gln at field strengths lower than 7T is difficult. However, we simulated the effects of increases in Gln and decreases in Glu using GAMMA (137). From these simulations, measured line shapes of the Glx peaks and comparisons with the *in vitro* MR spectra, we were able to assign an increase in Gln and decrease in Glu to R6/2 mice (39). This feature, of decreased NAA and Glu and increased Gln, seems to be consistent with neurodegeneration in general. As well as being noted in the AD and HD models, it has also been found in other models of neurodegeneration, such as toxic lesions generated with, for instance, quinolinic acid (72).

Another study of R6/2 mice used HRMAS and *in vitro* MRS of urine and plasma to assess metabolic defects (138). The results were generally consistent with previous studies showing increased Gln and taurine in a number of

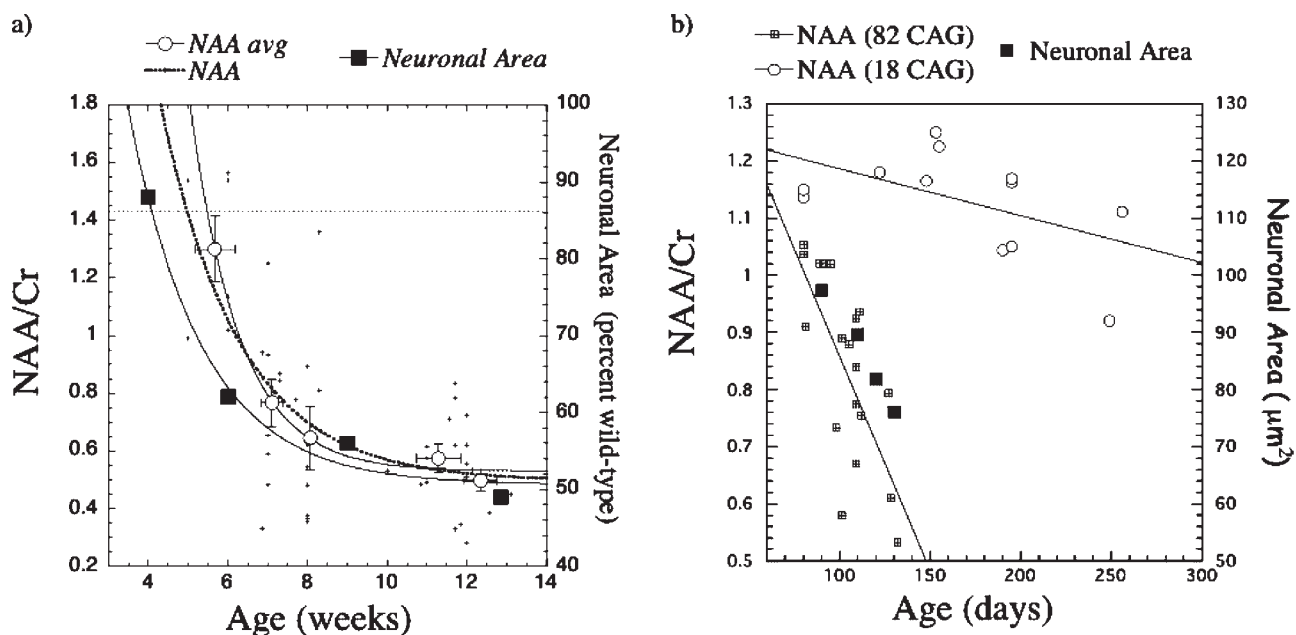


**Figure 7.** (a) Neuronal area and NAA concentrations in the striatum as a function of time in R6/2 mice (150 CAG repeats). Note that both neuronal area and NAA show an exponential decrease. (b) Comparison of neuronal area in mice with 82 and 18 CAG repeats over time with NAA measurements. In these two less severe phenotypes, NAA (and neuronal area) shows a linear decrease with age.

brain regions, as well as decreased NAA and Glu. This study also found increased glucose. The presence of acetate in a number of the spectra raises questions about sample handling. This study used a variety of statistical methods based on principle components analysis to discriminate between the wild-type and HD animals. Such studies show the value of high field strength (whether *in vivo* or *in vitro*) where so many different metabolites can be measured.

## PARKINSON'S DISEASE MODELS

PD is one of the few neurodegenerative disorders that can be reproduced fairly accurately using a toxin model. The toxin, MPTP, replicates almost all the pathological features of PD consequent on dopamine receptor loss, with the possible exception of Lewy bodies. A number of spectroscopic studies of PD have been reported in patients and animal models. The results in patients have been somewhat mixed, with some studies reporting little difference between PD and controls and others finding large differences. One of the problems is that the brain region most affected by PD is the substantia nigra, a region that is quite small with high iron content. As dopamine neurons make up only about 5% of the total neurons in the striatum (the projections from the nigra), at first glance it would appear that loss of these neurons would be difficult to detect using MRS. However, if there are metabolic changes consequent on loss of dopamine neurons, then changes might be detected. One recent study at 4 T showed no change in NAA in the nigra (139). On the other hand, toxin models have tended to show more change than observed in patients. We showed in a monkey model that there was a small loss of NAA subsequent to chronic, low-dose MPTP treatment, which progressed with time in concert with progressive loss of the dopamine transporter (a marker for pre-synaptic dopamine input) (140). A recent study used spectroscopic imaging to examine therapeutic interventions in MPTP-treated mice (141). Chemical shift imaging data with voxels approximately 1  $\mu$ L in volume were collected. Protection against MPTP-induced toxicity using injection of lymph cells from mice immunized with the chemical copolymer-1 (Cop-1) was demonstrated. The proposed mechanism of action is that Cop-1 induces autoimmune T-cells, preventing additional degeneration of the central nervous system, possibly through anti-inflammatory mechanisms. It remains to be seen how practical such studies of protection can become.

## INTERPRETATION OF SPECTROSCOPIC RESULTS

There are common threads that run through the interpretation of the data obtained in the mouse models

of neurodegeneration. Clearly, to no one's surprise, NAA is proving to be a useful model for neuronal dysfunction and loss, and has proved useful for following several therapeutic interventions. This has been validated in a number of studies. The roles of the other molecules were discussed above. One possible interpretation that seems consistent with a number of the conclusions about the neurodegenerative models is a change in the glial/neuronal balance. Glial cells possess more *myo*-inositol and Gln and little NAA, whereas neurons have large concentrations of NAA and more Glu. Thus a change in the neuronal/glial volume balance could lead to observations of decreased NAA and Glu, and increased Gln. This is illustrated in the Fig. 8. We took concentrations from cell culture data of a variety of sources for glial and neuronal cells. Unfortunately, cell cultures are probably not representative of the metabolic situation *in vivo*, but there is no way to separate the MRS signals *in vivo* from the glial and neuronal cells. The changes in the relative concentrations of selected chemicals are presented as a function of changing the neuronal/glial volume ratio. It can be seen that the general features observed in the neurodegenerative models above are noted. By measurement of the various metabolite ratios, it may be possible to assess this balance. For instance, in comparing the R6/2 mice with wild-type, we correlated the ratios from Fig. 8 (including a number of other chemicals) with those determined from the *in vitro* spectra. On the basis of maximizing the correlation

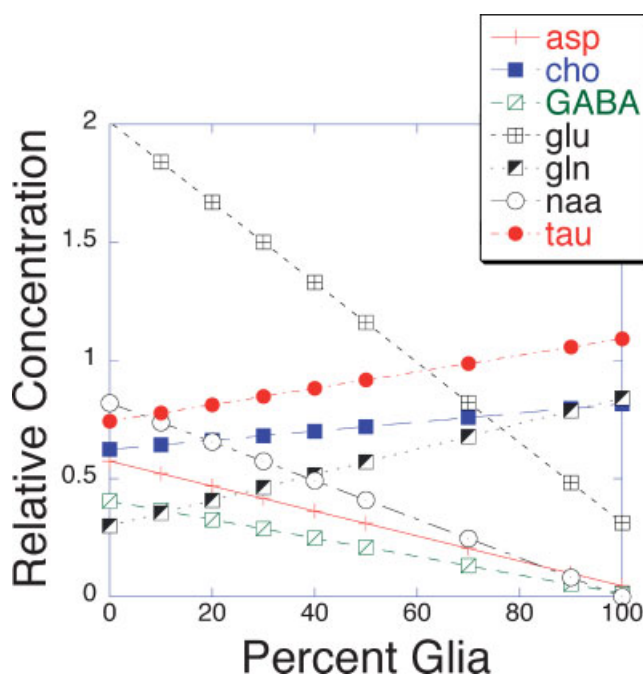


**Figure 8.** Changes in normalized neurochemical concentration ratios as a function of the ratio of glial/neuronal volume using data from *in vitro* cultured neurons and astrocytes from a variety of sources. By correlation of the observed ratios with those determined here, the glial/neuronal volume balance can potentially be estimated.

coefficient, the data suggest that the glial/neuronal volume ratio is about 50–60% neuronal in the wild-type and about 35–45% neuronal in the HD model. This would accord with the neuronal shrinkage noted above.

Other possible interpretations are altered glial–neuronal cycling, which is something that can be readily assessed using  $^{13}\text{C}$  MRS. Increased metabolism in general may lead to increased Glu and Gln (or Glx). One very interesting paper showed that, in patients with epilepsy, there was good correlation between PET measurements of 2- $^{18}\text{F}$ fluorodeoxy-D-glucose uptake and Glx measurements using MRS (142). The implication was that increased Glx could be interpreted as an increase in glucose metabolism. Obviously, this is a far less sophisticated measure than can be obtained using  $^{13}\text{C}$  MRS, but has the advantage of being readily available and easier to measure than the carbon studies. Correlations were noted between decreased Glu metabolism measured using  $^{13}\text{C}$  MRS and NAA in a small number of patients with AD, suggesting the utility of  $^{13}\text{C}$  NMR in AD studies (103).

## SUMMARY

MRS shows great promise for the study of mouse models of neurodegeneration. In addition to its role in understanding fundamental changes in the neurochemistry relevant to etiological mechanisms such as excitotoxicity, MRS may prove most useful in longitudinal monitoring of potential therapeutic interventions. The efficiency with which mice can be used for this purpose, combined with the non-invasive nature of MRS, makes it a powerful means of performing translational studies. Further, the different tissue compartments and neurochemical pathways represented by the various chemicals observable by MRS mean that multiple components of the neurodegenerative cascade can be studied. Other complementary techniques, such as histology, genetics, behavioral testing, are still required to allow the different neurochemicals to become true ‘biomarkers’ that could potentially be used as surrogate end points for therapeutic trials.

## Acknowledgements

We acknowledge the contributions of our many colleagues to the work presented here: in particular, Drs Ole Andreassen, M. Flint Beal, Iris Chen, Ekkehardt Kuestermann, Russell Matthews, Diana Rosas and Bruce Rosen.

## REFERENCES

- MacDonald ME, Gusella JF. Huntington's disease: translating a CAG repeat into a pathogenic mechanism. *Curr Opin Neurobiol* 1996; **6**: 638–643.
- Ordway JM, Tallaksen-Greene S, Gutekunst CA, Bernstein EM, Cearley JA, Wiener HW, Dure LSt, Lindsey R, Hersch SM, Jope RS, Albin RL, Detloff PJ. Ectopically expressed CAG repeats cause intranuclear inclusions and a progressive late onset neurological phenotype in the mouse. *Cell* 1997; **91**: 753–763.
- Bossy-Wetzel E, Schwarzenbacher R, Lipton SA. Molecular pathways to neurodegeneration. *Nat Med* 2004; **10 Suppl**: S2–9.
- Kopito RR. Aggresomes, inclusion bodies and protein aggregation. *Trends Cell Biol* 2000; **10**: 524–530.
- Ross CA, Poirier MA. Opinion: What is the role of protein aggregation in neurodegeneration? *Nat Rev Mol Cell Biol* 2005; **6**: 891–898.
- Schulz JB, Dichgans J. Molecular pathogenesis of movement disorders: are protein aggregates a common link in neuronal degeneration? *Curr Opin Neurol* 1999; **12**: 433–439.
- Fisher M. Potentially effective therapies for acute ischemic stroke. *Eur Neurol* 1995; **35**: 3–7.
- Hossmann KA. Glutamate-mediated injury in focal cerebral ischemia: the excitotoxic hypothesis revised. *Brain Pathol* 1994; **4**: 23–36.
- Hossmann KA. Pathophysiology and therapy of experimental stroke. *Cell Mol Neurobiol* 2006.
- Keller JN, Kindy MS, Holtsberg FW, St Clair DK, Yen HC, Germeyer A, Steiner SM, Bruce-Keller AJ, Hutchins JB, Mattson MP. Mitochondrial manganese superoxide dismutase prevents neural apoptosis and reduces ischemic brain injury: suppression of peroxynitrite production, lipid peroxidation, and mitochondrial dysfunction. *J Neurosci* 1998; **18**: 687–697.
- Kogure T, Kogure K. Molecular and biochemical events within the brain subjected to cerebral ischemia (targets for therapeutical intervention). *Clin Neurosci* 1997; **4**: 179–183.
- Siesjo BK. Pathophysiology and treatment of focal cerebral ischemia. Part II: Mechanisms of damage and treatment. *J Neurosurg* 1992; **77**: 337–354.
- Beal MF, Henshaw DR, Jenkins BG, Rosen BR, Schulz JB. Coenzyme Q10 and nicotinamide block striatal lesions produced by the mitochondrial toxin malonate. *Ann Neurol* 1994; **36**: 882–888.
- Jenkins B, Chen Y, Rosen B (eds). *Investigating the neurochemistry and etiology of neurodegenerative disorders using magnetic resonance spectroscopy*. Wiley-Liss: New York, 1997.
- Jenkins BG, Brouillet E, Chen YC, Storey E, Schulz JB, Kirschner P, Beal MF, Rosen BR. Non-invasive neurochemical analysis of focal excitotoxic lesions in models of neurodegenerative illness using spectroscopic imaging. *J Cereb Blood Flow Metab* 1996; **16**: 450–461.
- Blass JP, Sheu RK, Cedarbaum JM. Energy metabolism in disorders of the nervous system. *Rev Neurol* 1988; **144**: 543–563.
- Chou SY, Lee YC, Chen HM, Chiang MC, Lai HL, Chang HH, Wu YC, Sun CN, Chien CL, Lin YS, Wang SC, Tung YY, Chang C, Chern Y. CGS21680 attenuates symptoms of Huntington's disease in a transgenic mouse model. *J Neurochem* 2005; **93**: 310–320.
- Andreassen OA, Dedeoglu A, Ferrante RJ, Jenkins BG, Ferrante KL, Thomas M, Friedlich A, Browne SE, Schilling G, Borchelt DR, Hersch SM, Ross CA, Beal MF. Creatine increases survival and delays motor symptoms in a transgenic animal model of Huntington's disease. *Neurobiol Dis* 2001; **8**: 479–491.
- Ferrante RJ, Andreassen OA, Jenkins BG, Dedeoglu A, Kummerle S, Kubilus JK, Kaddurah-Daouk R, Hersch SM, Beal MF. Neuroprotective effects of creatine in a transgenic mouse model of Huntington's disease. *J Neurosci* 2000; **20**: 4389–4397.
- Choi IY, Lee SP, Guilfoyle DN, Helpert JA. *In vivo* NMR studies of neurodegenerative diseases in transgenic and rodent models. *Neurochem Res* 2003; **28**: 987–1001.
- Hilal SK, Maudsley AA, Simon HE, Perman WH, Bonn J, Mawad ME, Silver AJ, Ganti SR, Sane P, Chien IC. *In vivo* NMR imaging of tissue sodium in the intact cat before and after acute cerebral stroke. *AJNR Am J Neuroradiol* 1983; **4**: 245–249.
- Kalyanapuram R, Seshan V, Bansal N. Three-dimensional triple-quantum-filtered  $^{23}\text{Na}$  imaging of the dog head *in vivo*. *J Magn Reson Imaging* 1998; **8**: 1182–1189.

23. Lin SP, Song SK, Miller JP, Ackerman JJ, Neil JJ. Direct, longitudinal comparison of (1)H and (23)Na MRI after transient focal cerebral ischemia. *Stroke* 2001; **32**: 925–932.
24. Thulborn KR, Gindin TS, Davis D, Erb P. Comprehensive MR imaging protocol for stroke management: tissue sodium concentration as a measure of tissue viability in nonhuman primate studies and in clinical studies. *Radiology* 1999; **213**: 156–166.
25. Pfeuffer J, Tkac I, Provencher SW, Gruetter R. Toward an *in vivo* neurochemical profile: quantification of 18 metabolites in short-echo-time (1)H NMR spectra of the rat brain. *J Magn Reson* 1999; **141**: 104–120.
26. Tkac I, Andersen P, Adriany G, Merkle H, Ugurbil K, Gruetter R. *In vivo* <sup>1</sup>H NMR spectroscopy of the human brain at 7 T. *Magn Reson Med* 2001; **46**: 451–456.
27. Frahm J, Bruhn H, Gyngell ML, Merboldt KD, Hanicke W, Sauter R. Localized proton NMR spectroscopy in different regions of the human brain *in vivo*. Relaxation times and concentrations of cerebral metabolites. *Magn Reson Med* 1989; **11**: 47–63.
28. Behar KL, Ogino T. Assignment of resonances in the <sup>1</sup>H spectrum of rat brain by two-dimensional shift correlated and J-resolved NMR spectroscopy. *Magn. Reson. Med.* 1991; **17**: 285–303.
29. Behar KL, Ogino T. Characterization of macromolecule resonances in the <sup>1</sup>H NMR spectrum of rat brain. *Magn Reson Med* 1993; **30**: 38–44.
30. Birken DL, Oldendorf WH. N-Acetyl-L-aspartic acid: a literature review of a compound prominent in <sup>1</sup>H-NMR spectroscopic studies of brain. *Neurosci. Biobehav Rev.* 1989; **13**: 23–31.
31. Simmons ML, Frondoza CG, Coyle JT. Immunocytochemical localization of N-acetyl-aspartate with monoclonal antibodies. *Neuroscience* 1991; **45**: 37–45.
32. Urenjak J, Williams SR, Gadian DG, Noble M. Specific expression of N-acetyl-aspartate in neurons, oligodendrocyte-type-2 astrocyte progenitors, and immature oligodendrocytes *in vitro*. *J Neurochem* 1992; **59**: 55–61.
33. Urenjak J, Williams SR, Gadian DG, Noble M. Proton nuclear magnetic resonance spectroscopy unambiguously identifies different neural cell types. *J Neurosci* 1993; **13**: 981–989.
34. Hetherington HP, Pan JW, Mason GF, Adams D, Vaughn MJ, Twieg DB, Pohost GM. Quantitative <sup>1</sup>H spectroscopic imaging of human brain at 4.1 T using image segmentation. *Magn Reson Med* 1996; **36**: 21–29.
35. Shonk TK, Moats RA, Michaelis T, Mandigo JC, Izumi J, Ross BD. Probable Alzheimer disease: diagnosis with proton MR spectroscopy [see comments]. *Radiology* 1995; **195**: 65–72.
36. Jenkins BG, Koroshetz WJ, Beal MF, Rosen BR. Evidence for impairment of energy metabolism *in vivo* in Huntington's disease using localized <sup>1</sup>H NMR spectroscopy. *Neurology* 1993; **43**: 2689–2695.
37. Jenkins BG, Rosas HD, Chen YC, Makabe T, Myers R, MacDonald M, Rosen BR, Beal MF, Koroshetz WJ. <sup>1</sup>H NMR spectroscopy studies of Huntington's disease: correlations with CAG repeat numbers. *Neurology* 1998; **50**: 1357–1365.
38. Dunlop DS, Mc Hale DM, Lajtha A. Decreased brain N-acetyl-aspartate in Huntington's disease. *Brain Res* 1992; **580**: 44–48.
39. Jenkins BG, Klivenyi P, Kustermann E, Andreassen OA, Ferrante RJ, Rosen BR, Beal MF. Nonlinear decrease over time in N-acetyl aspartate levels in the absence of neuronal loss and increases in glutamine and glucose in transgenic Huntington's disease mice. *J Neurochem* 2000; **74**: 2108–2119.
40. De Stefano N, Matthews PM, Arnold DL. Reversible decreases in N-acetyl-aspartate after acute brain injury. *Magn Reson Med* 1995; **34**: 721–727.
41. Mathews PM, Andermann F, Silver K, Karpati G, Arnold DL. Proton MR spectroscopic characterization of differences in regional brain metabolic abnormalities in mitochondrial encephalomyopathies. *Neurology* 1993; **43**: 2484–2490.
42. Fenstermacher MJ, Narayana PA. Serial proton magnetic resonance spectroscopy of ischemic brain injury in humans. *Invest Radiol* 1990; **25**: 1034–1039.
43. Higuchi T, Fernandez EJ, Maudsley AA, Shimizu H, Weiner MW, Weinstein PR. Mapping of lactate and N-acetyl-L-aspartate predicts infarction during acute focal ischemia: *in vivo* <sup>1</sup>H magnetic resonance spectroscopy in rats. *Neurosurgery* 1996; **38**: 121–129; discussion 129–130.
44. Saunders DE. MR spectroscopy in stroke. *Br Med Bull* 2000; **56**: 334–345.
45. Davie CA, Hawkins CP, Barker GJ, Brennan A, Tofts PS, Miller DH, McDonald WI. Serial proton magnetic resonance spectroscopy in acute multiple sclerosis lesions. *Brain* 1994; **117**: 49–58.
46. De Stefano N, Matthews PM, Narayanan S, Francis GS, Antel JP, Arnold DL. Axonal dysfunction and disability in a relapse of multiple sclerosis: longitudinal study of a patient. *Neurology* 1997; **49**: 1138–1141.
47. Kuzniecky R, Palmer C, Hugg J, Martin R, Sawrie S, Morawetz R, Faught E, Knowlton R. Magnetic resonance spectroscopic imaging in temporal lobe epilepsy: neuronal dysfunction or cell loss? *Arch Neurol* 2001; **58**: 2048–2053.
48. Petroff OA, Errante LD, Rothman DL, Kim JH, Spencer DD. Neuronal and glial metabolite content of the epileptogenic human hippocampus. *Ann Neurol* 2002; **52**: 635–642.
49. Jenkins BG, Andreassen OA, Dedeoglu A, Leavitt B, Hayden M, Borchelt D, Ross CA, Ferrante RJ, Beal MF. Effects of CAG repeat length, HTT protein length and protein context on cerebral metabolism measured using magnetic resonance spectroscopy in transgenic mouse models of Huntington's disease. *J Neurochem* 2005; **95**: 553–562.
50. Taylor DL, Davies SE, Obrenovitch TP, Doheny MH, Patsalos PN, Clark JB, Symon L. Investigation into the role of N-acetyl-aspartate in cerebral osmoregulation. *J Neurochem* 1995; **65**: 275–281.
51. Baslow MH. Evidence supporting a role for N-acetyl-L-aspartate as a molecular water pump in myelinated neurons in the central nervous system. An analytical review. *Neurochem Int* 2002; **40**: 295–300.
52. Baslow MH. Brain N-acetyl-aspartate as a molecular water pump and its role in the etiology of Canavan disease: a mechanistic explanation. *J Mol Neurosci* 2003; **21**: 185–190.
53. Choi IY, Gruetter R. Dynamic or inert metabolite? Turnover of N-acetyl aspartate and glutathione from D-[1-<sup>13</sup>C]glucose in the rat brain *in vivo*. *J Neurochem* 2004; **91**: 778–787.
54. Karelson G, Ziegler A, Kunnecke B, Seelig J. Feeding versus infusion: a novel approach to study the NAA metabolism in rat brain. *NMR Biomed* 2003; **16**: 413–423.
55. Moreno A, Ross BD, Bluml S. Direct determination of the N-acetyl-L-aspartate synthesis rate in the human brain by (13)C MRS and [1-(13)C]glucose infusion. *J Neurochem* 2001; **77**: 347–350.
56. Kalra S, Cashman NR, Genge A, Arnold DL. Recovery of N-acetyl-aspartate in corticomotor neurons of patients with ALS after riluzole therapy. *Neuroreport* 1998; **9**: 1757–1761.
57. Prichard J, Rothman D, Novotny E, Petroff O, Kuwabara T, Avison M, Howseman A, Hanstock C, Shulman R. Lactate rise detected by <sup>1</sup>H NMR in human visual cortex during physiologic stimulation. *Proc Natl Acad Sci USA* 1991; **88**: 5829–5831.
58. Schurr A, West CA, Rigor BM. Lactate-supported synaptic function in the rat hippocampal slice preparation. *Science* 1988; **240**: 1326–1328.
59. Magistretti PJ, Pellerin L. Regulation by neurotransmitters of glial energy metabolism. *Adv Exp Med Biol* 1997; **429**: 137–143.
60. Petroff OA, Graham GD, Blamire AM, al-Rayess M, Rothman DL, Fayad PB, Brass LM, Shulman RG, Prichard JW. Spectroscopic imaging of stroke in humans: histopathology correlates of spectral changes. *Neurology* 1992; **42**: 1349–1354.
61. Dager SR, Strauss WL, Marro KI, Richards TL, Metzger GD, Artru AA. Proton magnetic resonance spectroscopy investigation of hyperventilation in subjects with panic disorder and comparison subjects. *Am J Psychiatry* 1995; **152**: 666–672.
62. Sotak CH, Alger JR. A pitfall associated with lactate detection using stimulated-echo proton spectroscopy. *Magn Reson Med* 1991; **17**: 533–538.
63. Doble A. The role of excitotoxicity in neurodegenerative disease: implications for therapy. *Pharmacol Ther* 1999; **81**: 163–221.
64. Leavitt BR, van Raamsdonk JM, Shehadeh J, Fernandes H, Murphy Z, Graham RK, Wellington CL, Raymond LA, Hayden MR. Wild-type huntingtin protects neurons from excitotoxicity. *J Neurochem* 2006; **96**: 1121–1129.
65. Rego AC, Oliveira CR. Mitochondrial dysfunction and reactive oxygen species in excitotoxicity and apoptosis: implications for

- the pathogenesis of neurodegenerative diseases. *Neurochem Res* 2003; **28**: 1563–1574.
66. Schousboe A, Waagepetersen HS. Role of astrocytes in glutamate homeostasis: implications for excitotoxicity. *Neurotox Res* 2005; **8**: 221–225.
  67. Mason GF, Pan JW, Ponder SL, Twieg DB, Pohost GM, Hetherington HP. Detection of brain glutamate and glutamine in spectroscopic images at 4.1 T. *Magn Reson Med* 1994; **32**: 142–145.
  68. Bristol LA, Rothstein JD. Glutamate transporter gene expression in amyotrophic lateral sclerosis motor cortex. *Ann Neurol* 1996; **39**: 676–679.
  69. Rothstein JD, Van Kammen M, Levey AI, Martin LJ, Kuncl RW. Selective loss of glial glutamate transporter GLT-1 in amyotrophic lateral sclerosis. *Ann Neurol* 1995; **38**: 73–84.
  70. Piore EP, Majors AW, Mitumoto H, Nelson DR, Ng TC. <sup>1</sup>H-MRS evidence of neurodegeneration and excess glutamate + glutamine in ALS medulla. *Neurology* 1999; **53**: 71–79.
  71. Andreassen OA, Jenkins BG, Dedeoglu A, Ferrante KL, Bogdanov MB, Kaddurah-Daouk R, Beal MF. Increases in cortical glutamate concentrations in transgenic amyotrophic lateral sclerosis mice are attenuated by creatine supplementation. *J Neurochem* 2001; **77**: 383–390.
  72. Tkac I, Keene CD, Pfeuffer J, Low WC, Gruetter R. Metabolic changes in quinolinic acid-lesioned rat striatum detected non-invasively by *in vivo* (1)H NMR spectroscopy. *J Neurosci Res* 2001; **66**: 891–898.
  73. Jenkins BG, Kraft E. Magnetic resonance spectroscopy in toxic encephalopathy and neurodegeneration. *Curr Opin Neurol* 1999; **12**: 753–760.
  74. Petroff OA, Pleban LA, Spencer DD. Symbiosis between *in vivo* and *in vitro* NMR spectroscopy: the creatine, N-acetylaspartate, glutamate, and GABA content of the epileptic human brain. *Magn Reson Imaging* 1995; **13**: 1197–1211.
  75. Podo F. Tumour phospholipid metabolism. *NMR Biomed* 1999; **12**: 413–439.
  76. Smith JK, Castillo M, Kwock L. MR spectroscopy of brain tumors. *Magn Reson Imaging Clin N Am* 2003; **11**: 415–429. v–vi.
  77. Brand A, Richter-Landsberg C, Leibfritz D. Multinuclear NMR studies on the energy metabolism of glial and neuronal cells. *Dev Neurosci* 1993; **15**: 289–298.
  78. Thurston JH, Sherman WR, Hauhart RE, Klopper RF. myo-inositol: a newly identified nonnitrogenous osmoregulatory molecule in mammalian brain. *Pediatr Res* 1989; **26**: 482–485.
  79. Isaacks RE, Bender AS, Kim CY, Shi YF, Norenberg MD. Effect of ammonia and methionine sulfoximine on myo-inositol transport in cultured astrocytes. *Neurochem Res* 1999; **24**: 51–59.
  80. Klunk WE, Xu C, Panchalingam K, McClure RJ, Pettegrew JW. Quantitative <sup>1</sup>H and <sup>31</sup>P MRS of PCA extracts of postmortem Alzheimer's disease brain. *Neurobiol Aging* 1996; **17**: 349–357.
  81. Pettegrew JW, Klunk WE, Panchalingam K, McClure RJ, Stanley JA. Magnetic resonance spectroscopic changes in Alzheimer's disease. *Ann N Y Acad Sci* 1997; **826**: 282–306.
  82. Behar KL, Boehm D. Measurement of GABA following GABA-transaminase inhibition by gabaculine: a <sup>1</sup>H and <sup>31</sup>P NMR spectroscopic study of rat brain *in vivo*. *Magn Reson Med* 1994; **31**: 660–667.
  83. Provencher SW. Estimation of metabolite concentrations from localized *in vivo* proton NMR spectra. *Magn Reson Med* 1993; **30**: 672–679.
  84. Bartha R, Drost DJ, Williamson PC. Factors affecting the quantification of short echo *in vivo* <sup>1</sup>H MR spectra: prior knowledge, peak elimination, and filtering. *NMR Biomed* 1999; **12**: 205–216.
  85. Hwang JH, Graham GD, Behar KL, Alger JR, Prichard JW, Rothman DL. Short echo time proton magnetic resonance spectroscopic imaging of macromolecule and metabolite signal intensities in the human brain. *Magn Reson Med* 1996; **35**: 633–639.
  86. Marjanska M, Curran GL, Wengenack TM, Henry PG, Bliss RL, Poduslo JF, Jack CR Jr, Ugurbil K, Garwood M. Monitoring disease progression in transgenic mouse models of Alzheimer's disease with proton magnetic resonance spectroscopy. *Proc Natl Acad Sci U S A* 2005; **102**: 11906–11910.
  87. Marcucci F, Airolidi L, Mussini E. Brain level of N-acetyl-L-aspartate in different strains of mouse and rat. *J Neurochem* 1969; **16**: 272–273.
  88. Cheng LL, Ma MJ, Becerra L, Ptak T, Tracey I, Lackner A, Gonzalez RG. Quantitative neuropathology by high resolution magic angle spinning proton magnetic resonance spectroscopy. *Proc Natl Acad Sci USA* 1997; **94**: 6408–6413.
  89. de Graaf RA, Brown PB, Mason GF, Rothman DL, Behar KL. Detection of [1,6-<sup>13</sup>C<sub>2</sub>]-glucose metabolism in rat brain by *in vivo* <sup>1</sup>H-[<sup>13</sup>C]-NMR spectroscopy. *Magn Reson Med* 2003; **49**: 37–46.
  90. Henry PG, Roussel R, Vaufrey F, Dautry C, Bloch G. Semiselective POCE NMR spectroscopy. *Magn Reson Med* 2000; **44**: 395–400.
  91. Pan JW, Stein DT, Telang F, Lee JH, Shen J, Brown P, Cline G, Mason GF, Shulman GI, Rothman DL, Hetherington HP. Spectroscopic imaging of glutamate C4 turnover in human brain. *Magn Reson Med* 2000; **44**: 673–679.
  92. Golman K, Ardenkjaer-Larsen JH, Petersson JS, Mansson S, Leunbach I. Molecular imaging with endogenous substances. *Proc Natl Acad Sci USA* 2003; **100**: 10435–10439.
  93. Golman K, Zandt RI, Lerche M, Pehrson R, Ardenkjaer-Larsen JH. Metabolic imaging by hyperpolarized <sup>13</sup>C magnetic resonance imaging for *in vivo* tumor diagnosis. *Cancer Res* 2006; **66**: 10855–10860.
  94. Badar-Goffer RS, Bachelard HS, Morris PG. Cerebral metabolism of acetate and glucose studied by <sup>13</sup>C-n.m.r. spectroscopy. A technique for investigating metabolic compartmentation in the brain. *Biochem J* 1990; **266**: 133–139.
  95. Bluml S, Moreno-Torres A, Shic F, Nguy CH, Ross BD. Tricarboxylic acid cycle of glia in the *in vivo* human brain. *NMR Biomed* 2002; **15**: 1–5.
  96. Hassel B, Sonnewald U, Fonnum F. Glial-neuronal interactions as studied by cerebral metabolism of [2-<sup>13</sup>C]acetate and [1-<sup>13</sup>C]glucose: an *ex vivo* <sup>13</sup>C NMR spectroscopic study. *J Neurochem* 1995; **64**: 2773–2782.
  97. Lebon V, Petersen KF, Cline GW, Shen J, Mason GF, Dufour S, Behar KL, Shulman GI, Rothman DL. Astroglial contribution to brain energy metabolism in humans revealed by <sup>13</sup>C nuclear magnetic resonance spectroscopy: elucidation of the dominant pathway for neurotransmitter glutamate repletion and measurement of astrocytic oxidative metabolism. *J Neurosci* 2002; **22**: 1523–1531.
  98. Gruetter R, Novotny EJ, Boulware SD, Mason GF, Rothman DL, Shulman GI, Prichard JW, Shulman RG. Localized <sup>13</sup>C NMR spectroscopy in the human brain of amino acid labeling from D-[1-<sup>13</sup>C]glucose. *J Neurochem* 1994; **63**: 1377–1385.
  99. Mason GF, Behar KL, Rothman DL, Shulman RG. NMR determination of intracerebral glucose concentration and transport kinetics in rat brain. *J Cereb Blood Flow Metab* 1992; **12**: 448–455.
  100. Mason GF, Gruetter R, Rothman DL, Behar KL, Shulman RG, Novotny EJ. Simultaneous determination of the rates of the TCA cycle, glucose utilization, alpha-ketoglutarate/glutamate exchange, and glutamine synthesis in human brain by NMR. *J Cereb Blood Flow Metab* 1995; **15**: 12–25.
  101. Sibson NR, Dhankhar A, Mason GF, Behar KL, Rothman DL, Shulman RG. *In vivo* <sup>13</sup>C NMR measurements of cerebral glutamine synthesis as evidence for glutamate-glutamine cycling. *Proc Natl Acad Sci USA* 1997; **94**: 2699–2704.
  102. Van Zijl PC, Davis D, Eleff SM, Moonen CT, Parker RJ, Strong JM. Determination of cerebral glucose transport and metabolic kinetics by dynamic MR spectroscopy. *Am J Physiol* 1997; **273**: E1216–1227.
  103. Lin AP, Shic F, Enriquez C, Ross BD. Reduced glutamate neurotransmission in patients with Alzheimer's disease: an *in vivo* (13)C magnetic resonance spectroscopy study. *Magma* 2003; **16**: 29–42.
  104. Choi J-K, Kuestermann E, Andreassen OA, Beal MF, Jenkins BG. A tale of two mice: impaired glial-neuronal cycling in mouse models of Huntington's disease and amyotrophic lateral sclerosis. International Society of Magnetic Resonance in Medicine 11<sup>th</sup> Scientific Meeting and Exhibition. Toronto, Canada, 2003; 437.
  105. Tyson RL, Sutherland GR. Labeling of N-acetylaspartate and N-acetylaspartylglutamate in rat neocortex, hippocampus and cerebellum from [1-<sup>13</sup>C]glucose. *Neurosci Lett* 1998; **251**: 181–184.

106. Serles W, Li LM, Antel SB, Cendes F, Gotman J, Olivier A, Andermann F, Dubeau F, Arnold DL. Time course of postoperative recovery of N-acetyl-aspartate in temporal lobe epilepsy. *Epilepsia* 2001; **42**: 190–197.
107. Kalra S, Arnold DL, Cashman NR. Biological markers in the diagnosis and treatment of ALS. *J Neurol Sci* 1999; **165 Suppl 1**: S27–32.
108. Signoretti S, Marmarou A, Fatouros P, Hoyle R, Beaumont A, Sawauchi S, Bullock R, Young H. Application of chemical shift imaging for measurement of NAA in head injured patients. *Acta Neurochir Suppl* 2002; **81**: 373–375.
109. Jenkins BG, Burns L, Pakzaban P, Chen YI, Deacon T, Rosen BR, Brillault C, Isacson I. Spectroscopic studies of neurochemical changes in a primate model of neurodegeneration and neural transplantation. Society of Magnetic Resonance 2<sup>nd</sup> Annual Meeting. San Francisco, 1994; 1423.
110. Ross BD, Hoang TQ, Bluml S, Dubowitz D, Kopyov OV, Jacques DB, Lin A, Seymour K, Tan J. *In vivo* magnetic resonance spectroscopy of human fetal neural transplants. *NMR Biomed* 1999; **12**: 221–236.
111. Beal MF, Brouillet E, Jenkins B, Henshaw R, Rosen B, Hyman BT. Age-dependent striatal excitotoxic lesions produced by the endogenous mitochondrial inhibitor malonate. *J Neurochem* 1993; **61**: 1147–1150.
112. Dijkhuizen RM, van Lookeren Campagne M, Niendorf T, Dreher W, van der Toorn A, Hoehn-Berlage M, Verheul HB, Tulleken CA, Leibfritz D, Hossmann KA, Nicolay K. Status of the neonatal rat brain after NMDA-induced excitotoxic injury as measured by MRI, MRS and metabolic imaging. *NMR Biomed* 1996; **9**: 84–92.
113. Henshaw R, Jenkins BG, Schulz JB, Ferrante RJ, Kowall NW, Rosen BR, Beal MF. Malonate produces striatal lesions by indirect NMDA receptor activation. *Brain Res* 1994; **647**: 161–166.
114. Lee WT, Shen YZ, Chang C. Neuroprotective effect of lamotrigine and MK-801 on rat brain lesions induced by 3-nitropropionic acid: evaluation by magnetic resonance imaging and *in vivo* proton magnetic resonance spectroscopy. *Neuroscience* 2000; **95**: 89–95.
115. Storey E, Hyman BT, Jenkins B, Brouillet E, Miller JM, Rosen BR, Beal MF. 1-Methyl-4-phenylpyridinium produces excitotoxic lesions in rat striatum as a result of impairment of oxidative metabolism. *J Neurochem* 1992; **58**: 1975–1978.
116. Schulz JB, Henshaw DR, Siwek D, Jenkins BG, Ferrante RJ, Cipolloni PB, Kowall NW, Rosen BR, Beal MF. Involvement of free radicals in excitotoxicity *in vivo*. *J Neurochem* 1995; **64**: 2239–2247.
117. Schulz JB, Matthews RT, Jenkins BG, Brar P, Beal MF. Improved therapeutic window for treatment of histotoxic hypoxia with a free radical spin trap. *J Cereb Blood Flow Metab* 1995; **15**: 948–952.
118. Kirschner PB, Jenkins BG, Schulz JB, Finkelstein SP, Matthews RT, Rosen BR, Beal MF. NGF, BDNF and NT-5, but not NT-3 protect against MPP<sup>+</sup> toxicity and oxidative stress in neonatal animals. *Brain Res* 1996; **713**: 178–185.
119. Jenkins B, Brouillet E, Chen Y, Storey E, Schulz J, Kirschner P, Beal M, Rosen B. Non-Invasive neurochemical analysis of focal excitotoxic lesions in models of neurodegenerative illness using spectroscopic imaging. *J. Cereb. Blood Flow Metab* 1996; **16**: 450–461.
120. Matthews RT, Yang L, Jenkins BG, Ferrante RJ, Rosen BR, Kaddurah-Daouk R, Beal MF. Neuroprotective effects of creatine and cyclocreatine in animal models of Huntington's disease. *J Neurosci* 1998; **18**: 156–163.
121. McGowan E, Eriksen J, Hutton M. A decade of modeling Alzheimer's disease in transgenic mice. *Trends Genet* 2006; **22**: 281–289.
122. Dedeoglu A, Choi JK, Cormier K, Kowall NW, Jenkins BG. Magnetic resonance spectroscopic analysis of Alzheimer's disease mouse brain that express mutant human APP shows altered neurochemical profile. *Brain Res* 2004; **1012**: 60–65.
123. von Kienlin M, Kunnecke B, Metzger F, Steiner G, Richards JG, Ozmen L, Jacobsen H, Loetscher H. Altered metabolic profile in the frontal cortex of PS2APP transgenic mice, monitored throughout their life span. *Neurobiol Dis* 2005; **18**: 32–39.
124. Oddo S, Caccamo A, Shepherd JD, Murphy MP, Golde TE, Kaye R, Metherate R, Mattson MP, Akbari Y, LaFerla FM. Triple-transgenic model of Alzheimer's disease with plaques and tangles: intracellular Abeta and synaptic dysfunction. *Neuron* 2003; **39**: 409–421.
125. Jenkins BG, Chen YI, Kuestermann E, Makris NM, Nguyen TV, Kraft E, Brownell AL, Rosas HD, Kennedy DN, Rosen BR, Koroshetz WJ, Beal MF. An integrated strategy for evaluation of metabolic and oxidative defects in neurodegenerative illness using magnetic resonance techniques [In Process Citation]. *Ann N Y Acad Sci* 1999; **893**: 214–242.
126. Jack CR Jr, Wengenack TM, Reyes DA, Garwood M, Curran GL, Borowski BJ, Lin J, Preboske GM, Holasek SS, Adriany G, Poduslo JF. *In vivo* magnetic resonance microimaging of individual amyloid plaques in Alzheimer's transgenic mice. *J Neurosci* 2005; **25**: 10041–10048.
127. Wu EX, Tang H, Asai T, Yan SD. Regional cerebral blood volume reduction in transgenic mutant APP (V717F, K670N/M671L) mice. *Neurosci Lett* 2004; **365**: 223–227.
128. Hoang TQ, Bluml S, Dubowitz DJ, Moats R, Kopyov O, Jacques D, Ross BD. Quantitative proton-decoupled <sup>31</sup>P MRS and <sup>1</sup>H MRS in the evaluation of Huntington's and Parkinson's diseases. *Neurology* 1998; **50**: 1033–1040.
129. Sanchez-Pernate R, Garcia-Segura JM, del Barrio Alba A, Viano J, de Yébenes JG. Clinical correlation of striatal <sup>1</sup>H MRS changes in Huntington's disease. *Neurology* 1999; **53**: 806–812.
130. Harms L, Meierkord H, Timm G, Pfeiffer L, Ludolph AC. Decreased N-acetyl-aspartate/choline ratio and increased lactate in the frontal lobe of patients with Huntington's disease: a proton magnetic resonance spectroscopy study. *J Neurol Neurosurg Psychiatry* 1997; **62**: 27–30.
131. Mangiarini L, Sathasivam K, Seller M, Cozens B, Harper A, Hetherington C, Lawton M, Trotter Y, Leach H, Davies SW, Bates GP. Exon 1 of the HD gene with an expanded CAG repeat is sufficient to cause a progressive neurological phenotype in transgenic mice. *Cell* 1996; **87**: 493–506.
132. Davies SW, Turmaine M, Cozens BA, DiFiglia M, Sharp AH, Ross CA, Scherzinger E, Wanker EE, Mangiarini L, Bates GP. Formation of neuronal intranuclear inclusions underlies the neurological dysfunction in mice transgenic for the HD mutation. *Cell* 1997; **90**: 537–548.
133. Schilling G, Becher MW, Sharp AH, Jinnah HA, Duan K, Kotzok JA, Slunt HH, Ratovitski T, Cooper JK, Jenkins NA, Copeland NG, Price DL, Ross CA, Borchelt DR. Intranuclear inclusions and neuritic aggregates in transgenic mice expressing a mutant N-terminal fragment of huntingtin [published erratum appears in *Hum Mol Genet* 1999 May; **8**(5): 943]. *Hum Mol Genet* 1999; **8**: 397–407.
134. Hodgson JG, Agopyan N, Gutekunst CA, Leavitt BR, LePiane F, Singaraja R, Smith DJ, Bissada N, McCutcheon K, Nasir J, Jamot L, Li XJ, Stevens ME, Rosemond E, Roder JC, Phillips AG, Rubin EM, Hersch SM, Hayden MR. A YAC mouse model for Huntington's disease with full-length mutant huntingtin, cytoplasmic toxicity, and selective striatal neurodegeneration. *Neuron* 1999; **23**: 181–192.
135. van Dellen A, Welch J, Dixon RM, Cordery P, York D, Styles P, Blakemore C, Hannan AJ. N-Acetylaspartate and DARPP-32 levels decrease in the corpus striatum of Huntington's disease mice. *Neuroreport* 2000; **11**: 3751–3757.
136. Law RO. Regulation of mammalian brain cell volume. *J Exp Zool* 1994; **268**: 90–96.
137. Smith SA, Levante TO, Meier BH, Ernst RR. Computer simulations in magnetic resonance. An object oriented programming approach. *J. Magn. Reson.* 1994; **106a**: 75–105.
138. Tsang TM, Woodman B, McLoughlin GA, Griffin JL, Tabrizi SJ, Bates GP, Holmes E. Metabolic characterization of the R6/2 transgenic mouse model of Huntington's disease by high-resolution MAS <sup>1</sup>H NMR spectroscopy. *J Proteome Res* 2006; **5**: 483–492.
139. Oz G, Terpstra M, Tkac I, Aia P, Lowary J, Tuite PJ, Gruetter R. Proton MRS of the unilateral substantia nigra in the human brain at 4 tesla: detection of high GABA concentrations. *Magn Reson Med* 2006; **55**: 296–301.
140. Brownell AL, Jenkins BG, Elmaleh DR, Deacon TW, Spealman RD, Isacson O. Combined PET/MRS brain studies show dynamic

- and long-term physiological changes in a primate model of Parkinson disease. *Nat Med* 1998; **4**: 1308–1312.
141. Boska MD, Lewis TB, Destache CJ, Benner EJ, Nelson JA, Uberti M, Mosley RL, Gendelman HE. Quantitative  $^1\text{H}$  magnetic resonance spectroscopic imaging determines therapeutic immunization efficacy in an animal model of Parkinson's disease. *J Neurosci* 2005; **25**: 1691–1700.
  142. Pfund Z, Chugani DC, Juhasz C, Muzik O, Chugani HT, Wilds IB, Seraji-Bozorgzad N, Moore GJ. Evidence for coupling between glucose metabolism and glutamate cycling using FDG PET and  $^1\text{H}$  magnetic resonance spectroscopy in patients with epilepsy. *J Cereb Blood Flow Metab* 2000; **20**: 871–878.
  143. Barbiroli B, Iotti S, Lodi R. Aspects of human bioenergetics as studied *in vivo* by magnetic resonance spectroscopy. *Biochimie* 1998; **80**: 847–853.
  144. Barbiroli B, Montagna P, Martinelli P, Lodi R, Iotti S, Cortelli P, Funicello R, Zaniol P. Defective brain energy metabolism shown by *in vivo*  $^{31}\text{P}$  MR spectroscopy in 28 patients with mitochondrial cytopathies. *J Cereb Blood Flow Metab* 1993; **13**: 469–474.
  145. Radda GK. Control, bioenergetics, and adaptation in health and disease: noninvasive biochemistry from nuclear magnetic resonance. *FASEB J* 1992; **6**: 3032–3038.
  146. De Stefano N, Matthews PM, Ford B, Genge A, Karpati G, Arnold DL. Short-term dichloroacetate treatment improves indices of cerebral metabolism in patients with mitochondrial disorders. *Neurology* 1995; **45**: 1193–1198.
  147. Gruetter R, Novotny EJ, Boulware SD, Rothman DL, Shulman RG.  $^1\text{H}$  NMR studies of glucose transport in the human brain. *J Cereb Blood Flow Metab* 1996; **16**: 427–438.
  148. Gyngell ML, Michaelis T, Horstmann D, Bruhn H, Hanicke W, Merboldt KD, Frahm J. Cerebral glucose is detectable by localized proton NMR spectroscopy in normal rat brain *in vivo*. *Magn Reson Med* 1991; **19**: 489–495.
  149. Rothman DL, Sibson NR, Hyder F, Shen J, Behar KL, Shulman RG. *In vivo* nuclear magnetic resonance spectroscopy studies of the relationship between the glutamate-glutamine neurotransmitter cycle and functional neuroenergetics [In Process Citation]. *Philos Trans R Soc Lond B Biol Sci* 1999; **354**: 1165–1177.
  150. Yudkoff M, Nissim I, Daikhin Y, Lin ZP, Nelson D, Pleasure D, Erecinska M. Brain glutamate metabolism: neuronal-astroglial relationships. *Dev Neurosci* 1993; **15**: 343–350.
  151. Ross BD, Bluml S. New aspects of brain physiology. *NMR Biomed* 1996; **9**: 279–296.
  152. Bates TE, Strangward M, Keelan J, Davey GP, Munro PM, Clark JB. Inhibition of N-acetylaspartate production: implications for  $^1\text{H}$  MRS studies *in vivo*. *Neuroreport* 1996; **7**: 1397–1400.
  153. Basser PJ, Pierpaoli C. Microstructural and physiological features of tissues elucidated by quantitative-diffusion-tensor MRI. *J Magn Reson B* 1996; **111**: 209–219.
  154. Dijkhuizen RM, de Graaf RA, Tulleken KA, Nicolay K. Changes in the diffusion of water and intracellular metabolites after excitotoxic injury and global ischemia in neonatal rat brain. *J Cereb Blood Flow Metab* 1999; **19**: 341–349.
  155. Makris N, Worth AJ, Sorensen AG, Papadimitriou GM, Wu O, Reese TG, Wedeen VJ, Davis TL, Stakes JW, Caviness VS, Kaplan E, Rosen BR, Pandya DN, Kennedy DN. Morphometry of *in vivo* human white matter association pathways with diffusion-weighted magnetic resonance imaging. *Ann Neurol* 1997; **42**: 951–962.
  156. Pierpaoli C, Jezzard P, Basser PJ, Barnett A, Di Chiro G. Diffusion tensor MR imaging of the human brain. *Radiology* 1996; **201**: 637–648.
  157. Kermode AG, Thompson AJ, Tofts P, MacManus DG, Kendall BE, Kingsley DP, Moseley IF, Rudge P, McDonald WI. Breakdown of the blood-brain barrier precedes symptoms and other MRI signs of new lesions in multiple sclerosis. Pathogenetic and clinical implications. *Brain* 1990; **113**: 1477–1489.
  158. Tofts PS, Kermode AG. Measurement of the blood-brain barrier permeability and leakage space using dynamic MR imaging. *I. Fundamental concepts. Magn Reson Med* 1991; **17**: 357–367.
  159. Antonini A, Leenders KL, Meier D, Oertel WH, Boesiger P, Anliker M.  $T_2$  relaxation time in patients with Parkinson's disease. *Neurology* 1993; **43**: 697–700.
  160. Ordidge RJ, Gorell JM, Deniau JC, Knight RA, Helpert JA. Assessment of relative brain iron concentrations using  $T_2$ -weighted and  $T_2^*$ -weighted MRI at 3 Tesla. *Magn Reson Med* 1994; **32**: 335–341.
  161. Ye FQ, Martin WR, Allen PS. Estimation of brain iron *in vivo* by means of the interecho time dependence of image contrast. *Magn Reson Med* 1996; **36**: 153–158.
  162. Kwong KK, Belliveau JW, Chesler DA, Goldberg IE, Weisskoff RM, Poncelet BP, Kennedy DN, Hoppel BE, Cohen MS, Turner R, et al. Dynamic magnetic resonance imaging of human brain activity during primary sensory stimulation. *Proc Natl Acad Sci USA* 1992; **89**: 5675–5679.
  163. Ogawa S, Tank DW, Menon R, Ellermann JM, Kim SG, Merkle H, Ugurbil K. Intrinsic signal changes accompanying sensory stimulation: functional brain mapping with magnetic resonance imaging. *Proc Natl Acad Sci USA* 1992; **89**: 5951–5955.
  164. Bartenstein P, Weindl A, Spiegel S, Boecker H, Wenzel R, Ceballos-Baumann AO, Minoshima S, Conrad B. Central motor processing in Huntington's disease. A PET study. *Brain* 1997; **120** (Pt 9): 1553–1567.
  165. Belliveau JW, Kennedy DN Jr, McKinsty RC, Buchbinder BR, Weisskoff RM, Cohen MS, Vevea JM, Brady TJ, Rosen BR. Functional mapping of the human visual cortex by magnetic resonance imaging. *Science* 1991; **254**: 716–719.
  166. Detre JA, Leigh JS, Williams DS, Koretsky AP. Perfusion imaging. *Magn Reson Med* 1992; **23**: 37–45.
  167. Nguyen TV, Brownell AL, Iris Chen YC, Livni E, Coyle JT, Rosen BR, Cavagna F, Jenkins BG. Detection of the effects of dopamine receptor supersensitivity using pharmacological MRI and correlations with PET. *Synapse* 2000; **36**: 57–65.
  168. Dautry C, Conde F, Brouillet E, Mittoux V, Beal MF, Bloch G, Hantraye P. Serial  $^1\text{H}$ -NMR spectroscopy study of metabolic impairment in primates chronically treated with the succinate dehydrogenase inhibitor 3-nitropropionic acid. *Neurobiol Dis* 1999; **6**: 259–268.
  169. Koga K, Mori A, Ohashi S, Kurihara N, Kitagawa H, Ishikawa M, Mitumoto Y, Nakai M. H MRS identifies lactate rise in the striatum of MPTP-treated C57BL/6 mice. *Eur J Neurosci* 2006; **23**: 1077–1081.
  170. Pioro EP, Wang Y, Moore JK, Ng TC, Trapp BD, Klinkosz B, Mitumoto H. Neuronal pathology in the wobbler mouse brain revealed by *in vivo* proton magnetic resonance spectroscopy and immunocytochemistry. *Neuroreport* 1998; **9**: 3041–3046.